Journal of Thermal Analysis and Calorimetry (2021) 145:829–849
https://doi.org/10.1007/s10973-020-10125-y

Multi-stage artificial neural network structure-based optimization of geothermal energy powered Kalina cycle

Merve Senturk Acar[1]

Received: 1 June 2020 / Accepted: 24 July 2020 / Published online: 10 August 2020

Abstract

In this study, the geothermal energy powered Kalina cycle (GEP-KC) was optimized by using a multi-stage artificial neural network (ANN) analysis. The ANN model was basically composed of two stages. The first stage has one network, and the second stage consists of three networks in this ANN model. The 365 GEP-KCs were designed for four variable parameters. These designs were analytically analyzed by means of thermodynamic and economic analysis. The obtained data were used for modeling of multi-stage ANN structure. This multi-stage ANN model was designed with the aim of maximizing net present value (NPV). Turbine inlet pressure, geothermal water outlet temperature at evaporator, condenser pressure and ammonia mass fraction were input parameters of the multi-stage ANN model. Energy efficiency and exergy efficiency of the GEP-KC were outputs of the first stage, and the NPV of the GEP-KC was the output of the third network of the second stage. The most suitable network structure for the optimization of GEP-KC was performed by using the Levenberg–Marquardt variant of back-propagation learning algorithm for multi-stage ANN. The cov, MPE, RMSE and R^2 values of multi-stage ANN were calculated as 2.558308, 1.077997189, 1.777658128 and 0.994693, respectively, for NPV. The calculated masses and biases of this structure were used to determine the optimum operating parameters of GEP-KC. The analytical findings of the NPV, energy and exergy efficiencies of the optimum GEP-KC model were, respectively, determined as 113.0732 M$, 6.7285% and 46.8701% in a high accuracy with the ANN results.

Keywords Kalina cycle · Geothermal energy · Artificial neural network · Energy · Exergy

List of symbols

ANN	Artificial neural network
b	Bias
C	Cost ($)
c	Specific heat (kJ kg^{-1} K^{-1})
cov	Coefficient of variation
CEPCI	Chemical Engineering Plant Cost Index
$\dot{E}x$	Exergy rate (kW)
GEP-KC	Geothermal energy powered Kalina cycle
h	Specific enthalpy (kJ kg^{-1})
$\dot{m}$	Mass flow (kg s^{-1})
MPE	Mean percentage error
NPV	Net present value
$\dot{Q}$	Heat power (W)
R^2	Percentage of absolute change
RMSE	Error of the square root
T	Temperature (K)
$\dot{W}$	Power (W)
ε	Exergy efficiency (%)
α	Ammonia mass fraction (%)
ψ	Specific exergy (kJ kg^{-1})
η	Energy efficiency (%)

Subscripts

b	Benefit
con	Condenser
ch	Chemical
cw	Cooling water
elec	Electricity
eva	Evaporator
g	Generator
gf	Geothermal fluid
i	Interest rate
ic	Investment cost
j	Discount rate
l	Liquid
m,i	Inlet mass flow
m,o	Outlet mass flow

✉ Merve Senturk Acar
merve.senturkacar@bilecik.edu.tr

[1] Mechanical Engineering Department, Engineering Faculty, Bilecik Seyh Edebali University, Bilecik, Turkey

mo	Maintenance and operating
ol	Life time of system
ncf	Net cash flow
p	Pump
ph	Physical
r	Recuperator
sc	Salvage cost
sys	System
t	Time (year)
tr	Turbine
0	Dead state

Introduction

Nowadays, due to the continuous decrease in the reserves of fossil fuels and their increasing environmental damage, studies are focused on generating power using renewable energy sources and heat sources such as waste heat recovery [1–4]. As geothermal energy is not affected by environmental conditions, it is one of the most preferred renewable energy sources in terms of sustainability [5, 6]. It is also important because of the absence of environmental pollutants due to the re-injection of the geothermal fluid after heat transfer. Due to these features, different energy systems where geothermal energy is used as a source are examined by researchers [7–10]. Organic Rankine cycle (ORC) and Kalina cycle (KC) are suitable for the power generation from low-temperature heat resources [11]. The difference between the ORC and the KC is that the ammonia-water mixture is used instead of the organic working fluid in KC [12]. In the heat exchangers of the ORC, there is a significant temperature mismatch between the heat sources and the working fluid, which reduces the performance of the cycle [11]. However, the ammonia-water mixture shows good temperature matching with the heat source, due to the temperature changes of mixture while the evaporation processes [13].

Thermodynamic and economic analysis is important in the modeling and optimization of energy systems [14–18]. In the literature, ammonia mass fraction, turbine inlet temperature, turbine inlet pressure, condenser pressure and condenser temperature are the main parameters used in KC optimization by thermodynamic and economic analysis [19–24]. Rodríguez et al. [1] compared the geothermal energy powered ORC and KC according to thermodynamic and economic analysis. They mentioned that R-290 for ORC and the ammonia-water mixture of 84% of ammonia mass fraction for KC are the most effective working fluids from the point of view of economic analysis. Arslan [6] investigated optimum geothermal water outlet temperature at evaporator and ammonia mass fraction of the Kalina cycle system (KCS-34) according to the thermodynamic and life cycle cost (LCC) analysis. Desideri and Bidini [23] investigated the optimal parameters of geothermal power plants. They stated that the turbine inlet pressure and working fluid type were the potential optimization parameters of geothermal power plant. Meng et al. [24] compared KC, ORC and transcritical CO_2 power cycle, according to the thermodynamic and economic analysis. They mentioned that the best energy efficiency, exergy efficiency and net power output were determined for ORC, KC and transcritical CO_2 power cycle.

Researchers have developed a new modeling technique due to the long time and economic constraints in modeling energy systems and determining the properties of different materials. Curve fitting is a technique used to develop the equation of a curve or plane that best fits the given experimental or analytical data. For this purpose, curve fitting technique is used to develop an equation of a curve or plane that best fits the given experimental or analytical data [25, 26]. The use of techniques such as artificial neural network (ANN), support vector machine, fuzzy logic and genetic algorithms is a highly sensitive alternative to establish a correlation [26, 27]. Nowadays, there are many studies on developing different models and determining the most sensitive model by using many intelligence methods and optimization algorithms to solve complex problems in a shorter time and economically [26–35]. Parashar et al. [28] developed a multilayer perceptron ANN model for the prediction of dynamic viscosity of MXene-palm oil nanofluid by using experimental data. They mentioned that the multilayer perceptron ANN model results well matched with experimental data. Barewar et al. [29] investigated the thermal conductivity of glycol-based Ag/ZnO hybrid nanofluids with curve fitting and ANN. They stated that the ANN model has a higher accuracy than the curve fitting method. Sencan and Kalogirou [30] determined the vapor pressure of the fluid couples by using ANN.

ANN algorithm was used for modeling, optimization and predicting of energy systems and sources [31, 32]. Farzaneh-Gord et al. [33] modeled ANN structure to predict a temperature drop of natural gas during a throttling process. Toghyani et al. [34] used ANN-particle swarm optimization, imperialist competitive algorithm-ANN and alone ANN model to estimate the power and torque values of the Stirling engine. The results show that the most suitable method was ANN-particle swarm optimization according to statistical analysis and experimental data. Wang et al. [35] investigated the optimum thermodynamic parameters of the supercritical CO_2 power cycle by using a genetic algorithm (GA) and ANN. They stated that the estimation of thermodynamic parameters of the system was with good accuracy by ANN. Cao et al. [2] optimized the Kalina-Flash cycles by genetic algorithm. They determined that the Kalina-Flash cycles more effective than KC from a thermodynamic and economic point of view. Saffari et al. [36] used Artificial Bee Colony (ABC) algorithm for

the optimization of the Kalina cycle. Sadeghi et al. [37] investigated the optimum parameters of double-turbine KC by using the ABC algorithm. Also, they investigated the effect of ammonia mass fraction, mass flow rate of the mixture, inlet pressure and temperature of the first separator on the net power output. They stated that although the ABC algorithm could not select an appropriate random food source at the initial stage of finding the optimum thermal efficiency, it could then approach the optimum value. Arslan [38] used an artificial neural network for the optimization of geothermal energy powered KC and determined that the optimum ammonia mass fraction ranges from 80% to 90% for KCS-34.

Studies related to ANN show that ANN provides great convenience in system design and optimization studies. In order to increase the sensitivity of the ANN model, new studies are focused on multi-stage and multilayer ANN structures. These studies are rare in the literature. Arat and Arslan [39] investigated the optimum design parameters of district heating system aided by a geothermal heat pump by using multi-stage with the multilevel ANN model. They mentioned that the analytical results and multi-stage and multilevel ANN model results well-matched according to the statistical analysis. Tugcu and Arslan [40] used a multi-stage and multilevel ANN model for the optimization of geothermal energy-aided absorption refrigeration systems. They stated that the ANN results show high accuracy with the analytical results.

In this study, it is aimed to determine the optimum working parameters of the geothermal energy powered Kalina Cycle (GEP-KC) with maximizing the NPV by means of ANN for the given system optimization parameters as ammonia mass fraction, the geothermal water outlet temperature at the evaporator, turbine inlet and condenser pressures. For this purpose, a multi-stage and multilayer (multi-stage) ANN model is designed to increase the accuracy of optimization. The multi-stage ANN model has been created to increase optimization accuracy. The ANN model was basically composed of two stages. The first has a single network, and the second stage consists of three networks in this ANN model. Levenberg–Marquardt (LM), Pola–Ribiere conjugate gradient (CGP) and scaled conjugate gradient (SCG) variants of the back-propagation learning algorithm were handled to determine the most suitable model of ANN. Logarithmic sigmoid function was used as an activation function in the analyses. The statistical methods were used to determine the optimum multi-stage ANN model structure. Optimum operating parameters of GEP-KC were determined using the masses of the most appropriate model of a multi-stage ANN model. Also, the applicability of this multi-stage ANN model for the optimization of GEP-KC was validated analytically.

Material and method

The GEP-KC parameters are designed parametrically according to the geothermal energy heat source temperature, cooling water temperature and thermodynamic properties of the ammonia-water mixture. In the system designs, the thermodynamic properties of the geothermal source in the Simav region were used. Well properties of the Simav geothermal region are given in Table 1.

The geothermal fluid is supplied from 9 wells. The temperature of the geothermal fluid is 406.65 K and its mass flow rate is 462 kg s^{-1} [5, 6, 39–45]. GEP-KC flow diagram is given in Fig. 1.

Geothermal energy powered Kalina cycle

As seen in Fig. 1, the ammonia-water mixture enters the condenser (point 10) and gives the heat to the cooling water. The saturated liquid mixture enters the pump (point 1) and outlets at evaporator pressure (point 2). The working fluid takes the heat of the mixer exhaust stream at the recuperator. The preheated working fluid enters the evaporator at point 3 and takes the heat of the geothermal fluid. The saturated liquid-vapor mixture is separated into two different flows at the separator. One is the high ammonia concentration (strong solution) and vapor-phased stream (point 5) and the other is low ammonia concentration (weak solution) and liquid-phased stream (point 6). Superheated strong solution flow is expanded at the turbine (point 7) to produce power. At the same time, weak solution flow passes through the valve to expand the condenser pressure (point 8). And both weak solution and strong solution flows are mixed in the mixer and enter to the recuperator (point 9). And it gives the heat to the high-pressured working fluid (point 2–3). Turbine inlet pressure ($P_4 = P_5$), geothermal water outlet temperature at evaporator (T_{2b}), condenser pressure ($P_7 = P_{10}$) and ammonia mass fraction (α) were the system design variables. The properties of the system components and system design parameters are given in Tables 2 and 3, respectively.

Table 1 Well properties of Simav geothermal region [5, 6, 38–40]

	$\dot{m}$/kg s^{-1}	T/K
Ej-1	72	420.85
Ej-3	50	412.05
Ej-4	65	412.05
Ej-5	60	412.05
E-6	70	412.05
E-8	50	416.75
E-9	60	366.75
E-11	35	361.45

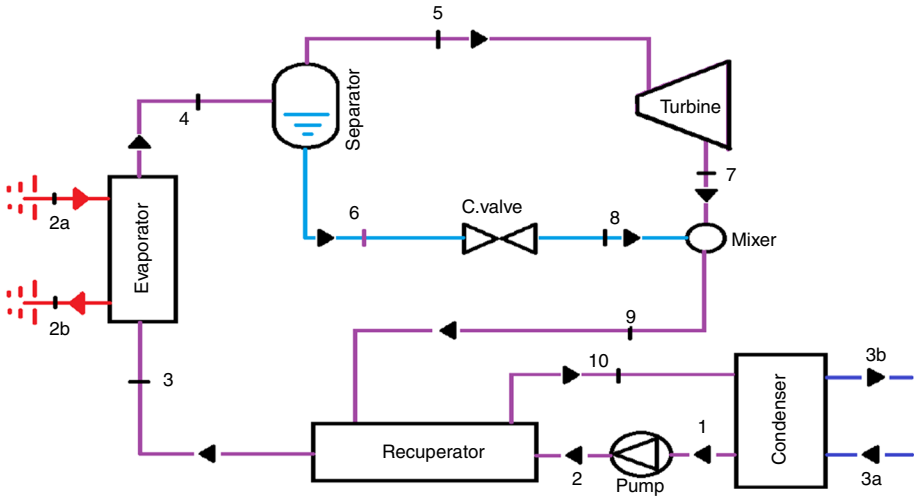

Fig. 1 Flow diagram of GEP-KC

Table 2 The properties of the system components

Component	Parameter	Values
Geothermal fluid	Inlet temperature T_{2a}	406.65 K
	Mass flow rate $\dot{m}_{2a}$	462 kg s^{-1}
Evaporator	Outlet temperature of working fluid T_4	398.15 K
	Effectiveness η_{eva}	0.85
Condenser	Inlet temperature T_{3a}	288.15 K
	Outlet temperature T_{3b}	298.15 K
	Pressure P_{cw}	4 kPa
	Effectiveness η_{con}	0.85
Turbine	Isentropic efficiency η_t	0.85
Pump	Isentropic efficiency η_p	0.80
Generator	Efficiency η_g	0.99
Recuperator	Effectiveness η_{rec}	0.85

The GEP-KC was designed for 90%, 85%, 80%, 75%, 70% of ammonia mass fraction (α). The thermodynamic properties of the ammonia-water mixture were determined by Reference Fluid Thermodynamic and Transport Properties Database 10.1 (REFPROP) [42].

Energy and exergy analysis

There are some assumptions such as kinetic and potential energy effects that are negligible, and the reference state is 298.15 K and 101.325 kPa in the thermodynamic analysis. The governing energy equations of the GEP-KC were obtained as given in Table 4.

The power output of the GEP-KC is

$$\dot{W}_{net} = \dot{W}_g - \dot{W}_p \tag{1}$$

The energy efficiency of the GEP-KC is calculated as

$$\eta = \frac{\dot{W}_{net}}{\dot{m}_{gf} \cdot c_{gf} \cdot T_{1a}} \tag{2}$$

The exergy balance equation for steady systems is given by the following equation:

$$\dot{E}_{X_{heat}} - \dot{E}_{X_{work}} + \dot{E}_{X_{m,i}} - \dot{E}_{X_{m,o}} = \dot{E}_{X_d} \tag{3}$$

where the exergy terms occurred by heat, work and mass flow exergies are given as follows;

$$\dot{E}_{X_{heat}} = \sum \left(1 - \frac{T_0}{T}\right) \cdot \dot{Q} \tag{4}$$

Table 3 The range of the system designing parameters

α (%)	$P_4 = P_5$/kPa	$P_7 = P_{10}$/kPa	T_{2b}/K
90	5808, 5308, 4808, 4308, 3808	1100, 1000, 900, 800, 700	373.15, 363.15, 353.15
85			
80			
75	4808, 4308, 3808, 3308, 2808		
70			

Table 4 Energy and exergy equations of the GEP-KC

Component	Energy equation	Exergy equation
Evaporator	$\dot{m}_{gf} \cdot (h_{2a} - h_{2b}) \cdot \eta_{eva} = \dot{m}_4 \cdot (h_4 - h_3)$	$\dot{m}_{gf} \cdot (\psi_{2a} - \psi_{2b}) + \dot{m}_4 \cdot (\psi_3 - \psi_4) = \dot{E}_{X_{d,eva}}$
Separator	$\dot{m}_4 \cdot h_4 = \dot{m}_5 \cdot h_5 + \dot{m}_6 \cdot h_6$	$\dot{m}_4 \cdot \psi_4 - \dot{m}_5 \cdot \psi_5 - \dot{m}_6 \cdot \psi_6 = \dot{E}_{X_{d,sep}}$
Turbine	$\dot{W}_{tr} = \dot{m}_5 \cdot (h_5 - h_7)$	$\dot{m}_5 \cdot \psi_5 - \dot{m}_7 \cdot \psi_7 - \dot{W}_{tr} = \dot{E}_{X_{d,tr}}$
Generator	$\dot{W}_g = \eta_g \cdot \dot{W}_{tr}$	$\dot{W}_{tr} - \dot{W}_g = \dot{E}_{X_{d,g}}$
Mixer	$\dot{m}_9 \cdot h_9 = \dot{m}_7 \cdot h_7 + \dot{m}_8 \cdot h_8$	$\dot{m}_7 \cdot \psi_7 + \dot{m}_8 \cdot \psi_8 - \dot{m}_9 \cdot \psi_9 = \dot{E}_{X_{d,mixer}}$
Recuperator	$\dot{m}_9 \cdot (h_9 - h_{10}) \cdot \eta_{rec} = \dot{m}_2 \cdot (h_3 - h_2)$	$\dot{m}_9 \cdot (\psi_9 - \psi_{10}) + \dot{m}_2 \cdot (\psi_2 - \psi_3) = \dot{E}_{X_{d,rec}}$
Condenser	$\dot{m}_{10} \cdot (h_{10} - h_1) \cdot \eta_{con} = \dot{m}_{cw} \cdot (h_{3b} - h_{3a})$	$\dot{m}_{10} \cdot (\psi_{10} - \psi_1) + \dot{m}_{cw} \cdot (\psi_{3a} - \psi_{3b}) = \dot{E}_{X_{d,con}}$
Pump	$\dot{W}_p = \dot{m}_2 \cdot (h_3 - h_2) = \dot{m}_2 \cdot (h_{3s} - h_2)/\eta_p$	$\dot{m}_2 \cdot (\psi_2 - \psi_3) + \dot{W}_p = \dot{E}_{X_{d,p}}$

$$\dot{E}_{X_{work}} = \dot{W} \tag{5}$$

$$\dot{E}_{X_{m,i}} = \sum \dot{m}_i \cdot \psi_i \tag{6}$$

$$\dot{E}_{X_{m,o}} = \sum \dot{m}_o \cdot \psi_o \tag{7}$$

here ψ indicates the physical and chemical exergy term and the physical exergy term is given as follows:

$$\psi = \psi_{ph} + \psi_{ch} \tag{8}$$

$$\psi_{ph} = (h - h_0) - T_0 \cdot (s - s_0) \tag{9}$$

where h is enthalpy, s is entropy, and the subscript zero indicates the properties of fluids at the dead state. The chemical exergy term is given as follows:

$$\psi_{ch} = \frac{\alpha}{M_{NH_3}} \cdot e^0_{ch,\,NH_3} - \frac{(1-\alpha)}{M_{H_2O}} \cdot e^0_{ch,\,H_2O} \tag{10}$$

where $e^0_{ch,\,NH_3}$ and $e^0_{ch,\,H_2O}$ are the molar exergy of the pure component at dead state conditions (kJ/mol), M is molar (kg/mol), x is mass ratio of ammonia in the mixture [43].

The exergetic efficiency of the system is then calculated by the following equation:

$$\varepsilon = 1 - \frac{\dot{E}_{X_{d,total}}}{\dot{E}_{X_{m,i}}} = \frac{\dot{W}_{net}}{(\dot{m}_{gf} \cdot (\psi_{2a} - \psi_{2b}))} \tag{11}$$

The governing energy and exergy equations of the GEP-KC were obtained as given in Table 4.

Economic analysis

The life cycle cost (C_{sys}) of GEP-KC occurs by the investment costs (C_{ic}), salvage cost (C_{sc}), maintenance and operating costs (C_{mo}) and benefit (C_b).

$$C_{sys} = C_b - (C_{ic} + C_{sc} + C_{mo}) \tag{12}$$

The salvage cost of GEP-KC was taken as 10% of the investment cost [44]. The maintenance and operating costs of GEP-KC system were taken as 6% of the investment cost of the GEP-KC [3].

The benefit of GEP-KC (C_b) includes electricity earning.

$$C_b = \dot{W}_{net} \cdot C_{elec} \cdot t_o \tag{13}$$

where C_{elec}; the unit price of electricity ($/kWh) and t_o; operating time of plant is 8400 h per annum [44]. C_{elec} is calculated by

$$C_{elec} = \frac{CEPCI_{2018}}{CEPCI_{2014}} \cdot C_{elec,2014} \tag{14}$$

where $C_{elec,\,2014}$; the unit price of electricity in 2014 is 0.06 $/kWh [29], $CEPCI_{2018}$; Chemical Engineering Plant Cost Index in 2018 is 603.1 [46] and $CEPCI_{2014}$; Chemical Engineering Plant Cost Index in 2014 is 576.1 [2].

The net cash flow (C_{ncf});

$$C_{ncf} = (C_b - C_{mo}) \cdot (1 + i)^{t-1} \tag{15}$$

here i is the interest rate and t is the related year time of cash flow. The net present value (NPV) of GEP-KC;

$$NPV = (C_{sc} - C_{ic}) + \sum_{t=0}^{ol} \frac{C_{ncf}}{(1+j)^t} \tag{16}$$

where ol; the lifetime of GEP-KC, j; the discount rate. In this study, the lifetime of GEP-KC system was added to calculations as 20 years. The discount and interest rates were taken as 18.5% and 19.5%, respectively [47]. The investment cost of GEP-KC is calculated by using module costing technique [2, 48]. The data used to calculate the purchase costs of the components were obtained from the literature in 2001 [48]. The equipment costs were modified for the year 2018 by

CEPCI. Chemical Engineering Plant Cost Index in 2001 is 397 [2].

Artificial neural network modeling

Artificial neural networks (ANN) are an information processing system that learns the events using external input and output information samples and determines how to produce solutions on the same problems. Artificial intelligence studies, which began in the first half of the 20th century, form the basis of artificial neural networks. In 1943, McCulloch and Pitts discussed the first mathematical model of the nerve cell [49]. Hebb, McCulloch and Pitts between 1940 and 1950 have shown that it is possible to formulate any logical expression with artificial neural networks. As a result of these studies, it has begun to make researches about artificial neural networks in the field of engineering [38, 49–52]. Today, artificial neural networks are widely used in the analysis of energy systems as in many engineering fields [55].

Artificial neural networks are mathematical models developed considering the general cognitive and neural biological structure of the human brain. Artificial neural network models are based on the following assumptions. The processing of information takes place in many simple elements called neurons. The basic structure of the neuron is shown in Fig. 2. Signals between neurons are transmitted over connections. As with all typical neural networks, each link has a respective mass that multiplies the transmitted signal. Each neuron applies the activation function (usually nonlinear) to the net input (sum of the weighted input signals) to determine its own output signal [52, 53].

Figure 2 shows the inputs (G_n), total function (Σ), masses (A_n), activation function (F) and output of the artificial neuron. The input is information from the artificial neuron. The masses show the effect of information from the artificial neuron on the neuron. The sum function calculates the net input from a neuron. By adding $G_0 = 1$ to the mass vector, the bias is incorporated into the artificial neuron structure. In this case, the bias functions as a mass. Net input (NG) since $A_{0l} = b_l$;

$$\mathrm{NG}_l = \sum_{i}^{n} G_i \cdot A_{il} + b_l \tag{17}$$

where n is the total number of inputs to a neuron, b is the bias and l indicates the output element. In artificial neural networks, various addition functions such as product, maximum, minimum, majority and cumulative sum are used. The activation function determines the output by processing the net input to the neuron. Different activation functions such as logarithmic sigmoid function, linear function, step function, sin function, threshold value function and hyperbolic tangent function are used as the activation function. The logarithmic sigmoid function is indicated by

$$F(\mathrm{NG}) = \frac{1}{1 + e^{-\mathrm{NG}}} \tag{18}$$

Output is the value determined by the activation function [52, 53].

ANNs are two types in terms of their architectural structures. First, feedforward neural networks, communication between neurons is transmitted through unidirectional connections from the input layer to the output layer. The second structure, feedback artificial neural networks, the neurons in the output or intermediate layers are transmitted as input or re-input to the neurons in the intermediate layers [51, 55].

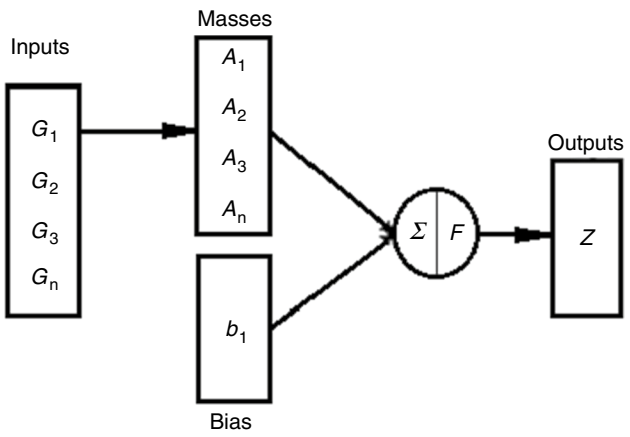

Fig. 2 Artificial neuron structure [54]

Statistical analysis of ANN

There are different learning algorithms used in ANN modeling. Although there are many learning algorithms used in the literature, Levenberg–Marquardt (LM) algorithm, Pola–Ribiere conjugate gradient (CGP) algorithm and scaled conjugate gradient (SCG) algorithm are widely used in the study of energy systems [38].

Learning performance of ANN is determined by using different statistical methods. The error of the square root (RMSE) is calculated by

$$\mathrm{RMSE} = \sqrt{\frac{\sum_{i=1}^{n} \left(\frac{z_{\mathrm{out}} - z_l}{z_{\mathrm{out}}} \right)^2}{n}} \tag{19}$$

here z_{ANN} is the output value of the ANN, z_l is the actual output value and n is the number of the values. The coefficient of variation (cov) is calculated with

$$\mathrm{cov} = \frac{\sum_{l=1}^{n}\left(z_{\mathrm{out}} - \bar{z}_{\mathrm{out}}\right)\cdot\left(z_{l} - \bar{z}_{l}\right)}{n}\cdot 100 \tag{20}$$

here $\bar{z}_{\mathrm{out}}$ is the average of the output set generated by the network and $\bar{z}_{l}$ is the average of the actual output set. The percentage of absolute change (R^2) is calculated by

$$R^2 = \left[\frac{\sum_{l=1}^{n}\left(z_{\mathrm{out}} - \bar{z}_{\mathrm{out}}\right)\cdot\left(z_{l} - \bar{z}_{l}\right)}{\sqrt{\sum_{l=1}^{n}\left(z_{\mathrm{out}} - \bar{z}_{\mathrm{out}}\right)^{2}\cdot\sum_{l=1}^{n}\left(z_{l} - \bar{z}_{l}\right)^{2}}}\right]^{2} \tag{21}$$

The mean percentage error (MPE) is calculated by

$$\mathrm{MPE} = \frac{\sum_{l=1}^{n}\left(z_{\mathrm{out}} - z_{l}\right)}{n.\left|z_{l,\max} - z_{l,\min}\right|}.100 \tag{22}$$

here $z_{l,\min}$ is the minimum value in the actual output set and $z_{l,\max}$ is the maximum value in the actual output set.

The error rates of the ANN results for optimum design are calculated as follows:

$$\mathrm{ER} = \frac{\left(z_{\mathrm{ANN}} - z_{\mathrm{analytic}}\right)}{z_{\mathrm{analytic}}}\cdot 100 \tag{23}$$

here z_{ANN} is the ANN result of the parameter and $z_{\mathrm{analytical}}$ is the analytical result of the parameter calculated for optimum system design.

Modeling of the GEP-KC system parameters by using multi-stage ann structure

ANN modeling was made by using the MATLAB computer program [56]. In this study, logarithmic sigmoid function, double layer network structure and supervised learning method were used in the ANN modeling. Network architectures were trained for 1000 iterations. The number of neurons in the hidden layer increased by two starting from four. Levenberg–Marquardt (LM) algorithm, Pola–Ribiere conjugate gradient (CGP) algorithm and scaled conjugate gradient (SCG) algorithm were used in ANNs.

The GEP-KC was designed for four variable parameters. Also, net present value (NPV), energy and exergy values of these models were determined analytically. These analytical results were used in the ANN analysis. Moreover, 70% of the designed models were used for training, and 30% of the designed models were used for testing. The multi-stage ANN model of GEP-KC is given in Fig. 3.

Turbine inlet pressure ($P_4 = P_5$), the geothermal water outlet temperature at the evaporator (T_{2b}), condenser pressure ($P_7 = P_{10}$) and ammonia mass fraction (α) were input parameters of the first and second stages of the ANN model. Energy (η) and exergy (ε) efficiencies of the GEP-KC were the output parameters of the first stage.

In the second stage, the inputs of second and third networks were the outputs of the previous network. The power output of the turbine ($\dot{W}_{\mathrm{tr}}$), the power input of the pump ($\dot{W}_{\mathrm{p}}$), the heat capacity of the evaporator ($\dot{Q}_{\mathrm{eva}}$), the heat capacity of the condenser ($\dot{Q}_{\mathrm{con}}$) and the heat capacity of the recuperator ($\dot{Q}_{\mathrm{rec}}$) were the output parameters of the first network and the input parameters of the second network in the second stage of the proposed ANN model. The investment cost (C_{ic}), the maintenance and operating costs (C_{mo}), the salvage cost (C_{sc}) and the benefit (C_{b})of the GEP-KC system were the output parameters of the second network and the input parameters of the third network in the second stage of the proposed ANN model. The NPV was the output of the third network in the second stage of the proposed multi-stage ANN model.

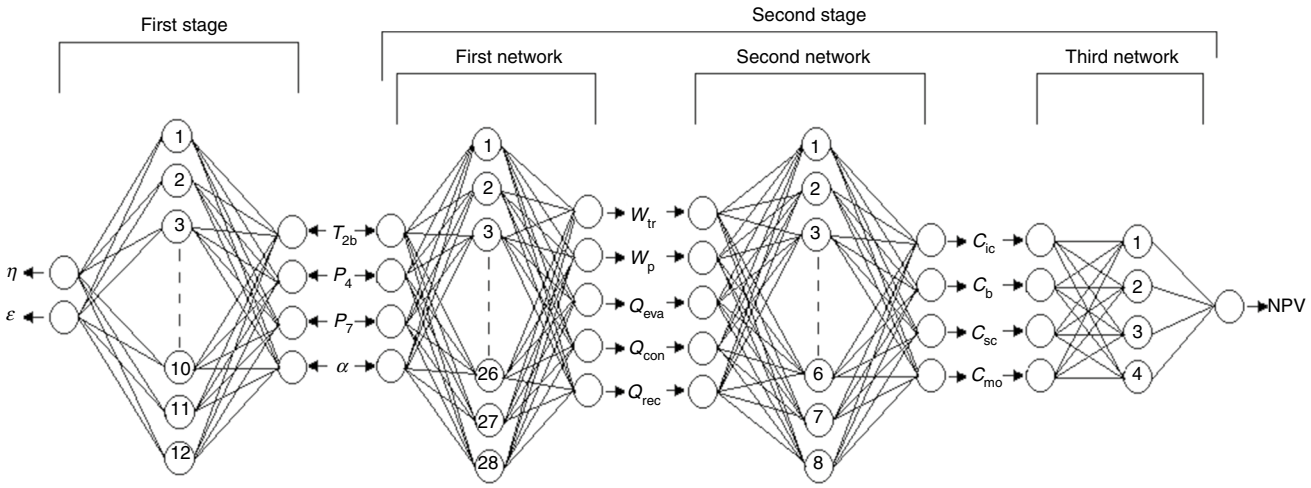

Fig. 3 Multi-stage ANN model of GEP-KC

In this ANN model, the first stage of network structure was used for evaluation of the input parameters of the first network of the second stage with energy and exergy analysis. The NPV value was maximized by the input parameters between the minimum and maximum values of the GEP-KC design parameters. The maximum value of the NPV was determined by using the structure that gave the most accurate results for each network, and the optimum values of the input parameters were determined. Finally, the system was analyzed analytically for the optimum system parameters which were determined by the ANN model and the results were compared statistically with the ANN results.

Results and discussion

In this study, 365 GEP-KC designs were built for different turbine inlet pressure (P_4=P_5), the geothermal water outlet temperature at the evaporator (T_{2b}), condenser pressure (P_7=P_{10}) and ammonia mass fraction (α). 255 of these designs were used for the training of network and 110 of them were used for testing. The energy and exergy efficiencies of the GEP-KC were the outputs of the first stage of the ANN model. The statistical results of the first stage outputs for different neurons and algorithms are given in Table 5.

As seen in Table 5, cov, MPE, RMSE and R^2 values of training results for energy efficiency change between 0.276928–6.573226, 0.206417–5.33857,

Table 5 The statistical results of first stage outputs

Parameter	Algorithm	Train				Test			
		cov	MPE	RMSE	R^2	cov	MPE	RMSE	R^2
η	LM 2-4	1.082833	0.897586	0.051816	0.996692	1.185262	1.001719	0.057681	0.996306
	LM 2-6	0.623575	0.482835	0.02984	0.998918	0.708355	0.601983	0.034472	0.99874
	LM 2-8	0.379419	0.275519	0.018156	0.999598	0.384578	0.329037	0.018715	0.999619
	LM 2-9	0.591006	0.481954	0.028281	0.99902	1.15391	0.70477	0.056155	0.996492
	LM 2-10	0.402286	0.313218	0.01925	0.999548	0.447271	0.373688	0.021766	0.999478
	LM 2-11	0.320017	0.251034	0.015314	0.999713	0.370425	0.315571	0.018027	0.999636
	LM 2-12	0.276928	0.206417	0.013252	0.999785	0.302137	0.237343	0.014703	0.999758
	LM 2-13	0.320463	0.24049	0.015335	0.999713	0.331355	0.297823	0.016125	0.999719
	LM 2-14	0.307375	0.251351	0.014709	0.999739	0.672399	0.35765	0.032722	0.998814
	CGP 2-4	6.573226	5.33857	0.314546	0.878549	6.324455	5.552956	0.307779	0.894313
	CGP 2-6	2.172266	1.71513	0.103949	0.986687	2.317154	2.047575	0.112764	0.985837
	CGP 2-7	1.991476	1.593255	0.095297	0.988822	2.378408	1.979787	0.115745	0.985038
	CGP 2-8	2.425707	1.987193	0.116076	0.983399	2.595712	2.250207	0.12632	0.982292
	SCG 2-4	4.790891	3.874221	0.229257	0.935243	4.897548	4.168767	0.238339	0.936647
	SCG 2-5	2.425821	1.92708	0.116082	0.983454	2.794302	2.331401	0.135985	0.979612
	SCG 2-6	5.898016	4.75857	0.282236	0.901855	6.158589	5.333871	0.299707	0.899433
ε	LM 2-4	3.878503	2.032297	1.240998	0.980800	3.850626	2.03732	1.253861	0.982839
	LM 2-6	2.380503	1.271515	0.761685	0.992767	2.623829	1.356406	0.854385	0.992023
	LM 2-8	1.077716	0.593071	0.344835	0.998518	1.259547	0.644561	0.41014	0.998204
	LM 2-9	1.179108	0.610325	0.377277	0.998228	7.923303	1.42762	2.580029	0.935919
	LM 2-10	1.217248	0.713629	0.389481	0.998109	1.58862	0.949841	0.517295	0.997077
	LM 2-11	0.854166	0.454782	0.273306	0.999073	1.128709	0.598763	0.367536	0.998544
	LM 2-12	0.296032	0.166644	0.094721	0.999888	0.40041	0.229608	0.130384	0.999814
	LM 2-13	0.698939	0.383869	0.223638	0.99938	1.050313	0.572807	0.342008	0.998812
	LM 2-14	0.731938	0.442012	0.234197	0.999355	5.350416	1.037658	1.742231	0.970145
	CGP 2-4	7.711541	4.703276	2.467449	0.924449	7.906874	4.927272	2.574679	0.928542
	CGP 2-6	5.03918	2.746217	1.612378	0.967591	5.345619	2.786212	1.740669	0.96747
	CGP 2-7	4.382582	2.334611	1.402287	0.975502	4.962838	2.524328	1.616026	0.971649
	CGP 2-8	4.770961	2.776664	1.526556	0.97095	5.2627	2.915787	1.713669	0.96808
	SCG 2-4	5.357884	3.439951	1.714353	0.963458	4.970152	3.118959	1.618408	0.971353
	SCG 2-5	5.155108	3.117512	1.649471	0.966141	5.024932	2.932342	1.636245	0.971249
	SCG 2-6	6.551904	4.079866	2.096402	0.945214	6.566397	4.127393	2.138185	0.950569

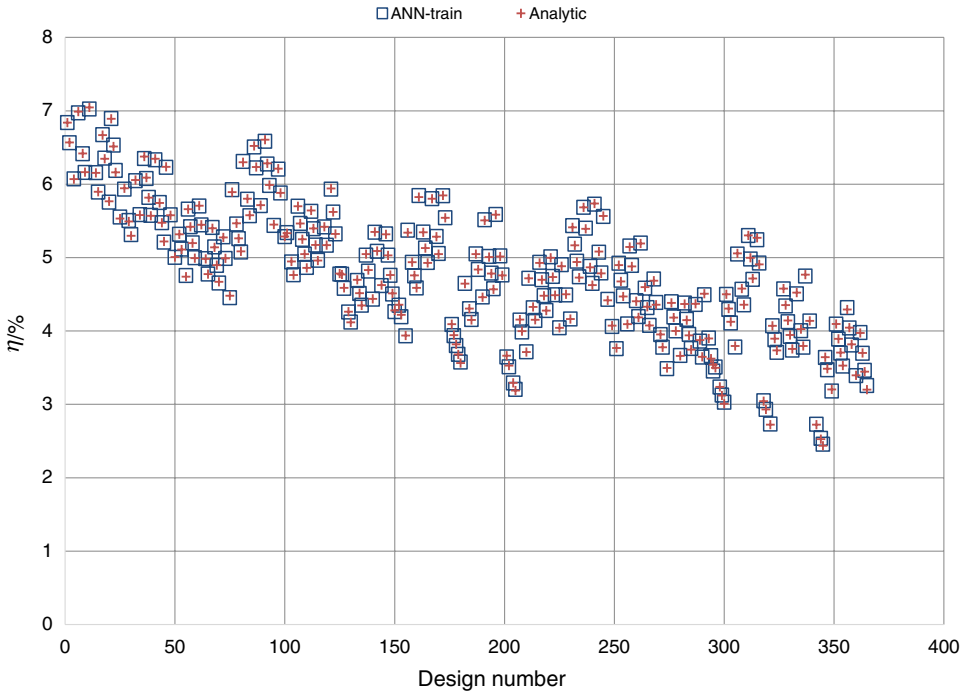

Fig. 4 Training and analytic results of energy efficiency

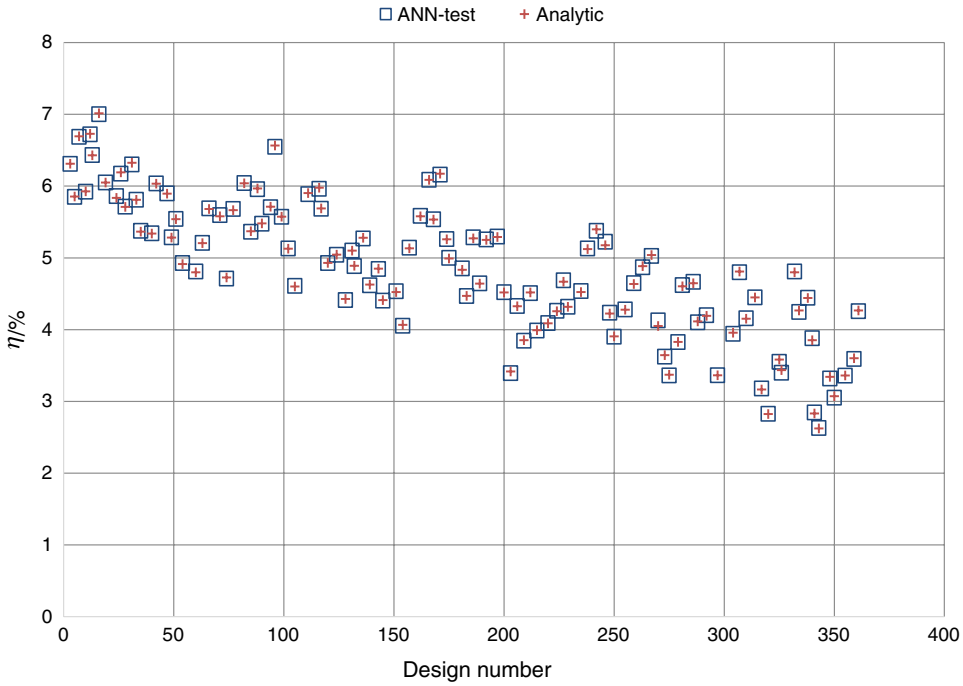

Fig. 5 Testing and analytic results of energy efficiency

0.013252–0.314546 and 0.901855–0.999785, respectively. The cov, MPE, RMSE and R^2 values of testing results for energy efficiency change between 0.302137–6.324455, 0.237343–5.552956, 0.014703–0.307779 and 0.899433–0.999758, respectively. The MPE, cov, RMSE and R^2 values of training results for exergy efficiency change between 0.166644–4.703276, 0.296032–7.711541, 0.094721–2.467449 and 0.924449–0.999888, respectively. The MPE, cov, RMSE and R^2 values of testing results for exergy efficiency change between 0.229608–4.927272, 0.40041–7.906874, 0.130384–2.574679 and 0.999814–0.928542, respectively. The results obtained from Table 5 show the optimum neuron values of the hidden layer as 12 based on the percentage of absolute change. The lowest values of MPE, cov, RMSE for energy and exergy efficiencies determination were observed with 12 neurons

in the hidden layer for training and testing results. The statistical results show that the most approximate algorithm and the number of neurons in the first stage are LM and 12, respectively. The ANN results and analytical results of energy efficiency are given in Figs. 4 and 5 for testing and training values.

As seen in Figs. 4 and 5, the analytical and LM 2-12 ANN model results of energy efficiency well coincided with each other. The MPE, cov, RMSE and R^2 values of training results for energy efficiency were obtained as 0.206417, 0.276928, 0.013252 and 0.999785, respectively, for LM 2-12 (Levenberg–Marquardt algorithm with one hidden layer with neuron values of 12) in training step. These values were obtained as 0.237343, 0.302137, 0.014703 and 0.999758, respectively, for LM 2-12 in the testing step. The exergy efficiency results are given in Figs. 6 and 7 for training and testing values of the LM 2-12 ANN model.

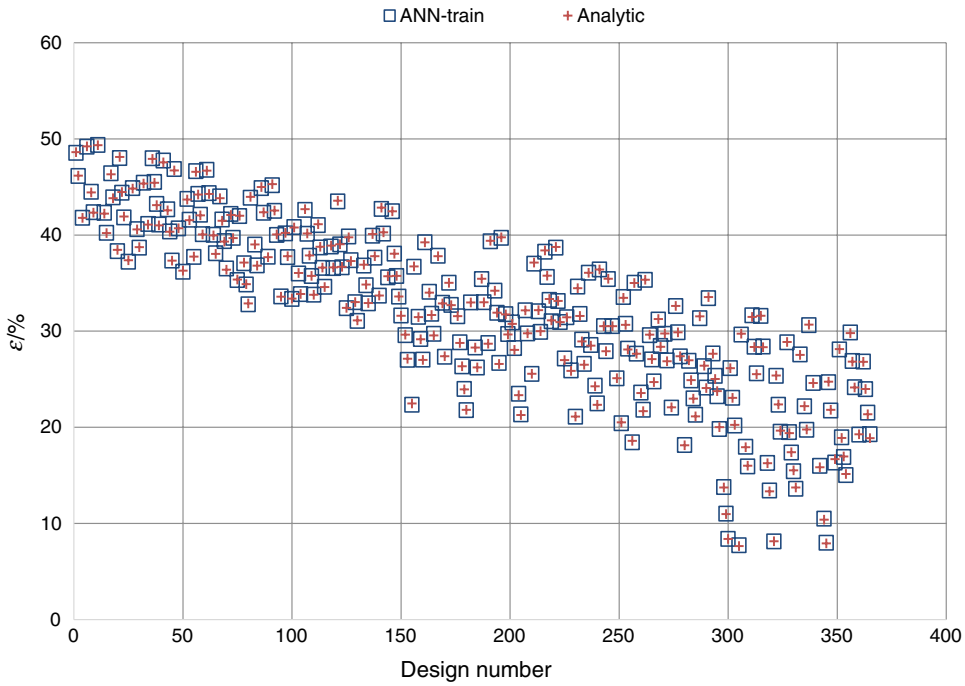

Fig. 6 Training and analytic results of exergy efficiency

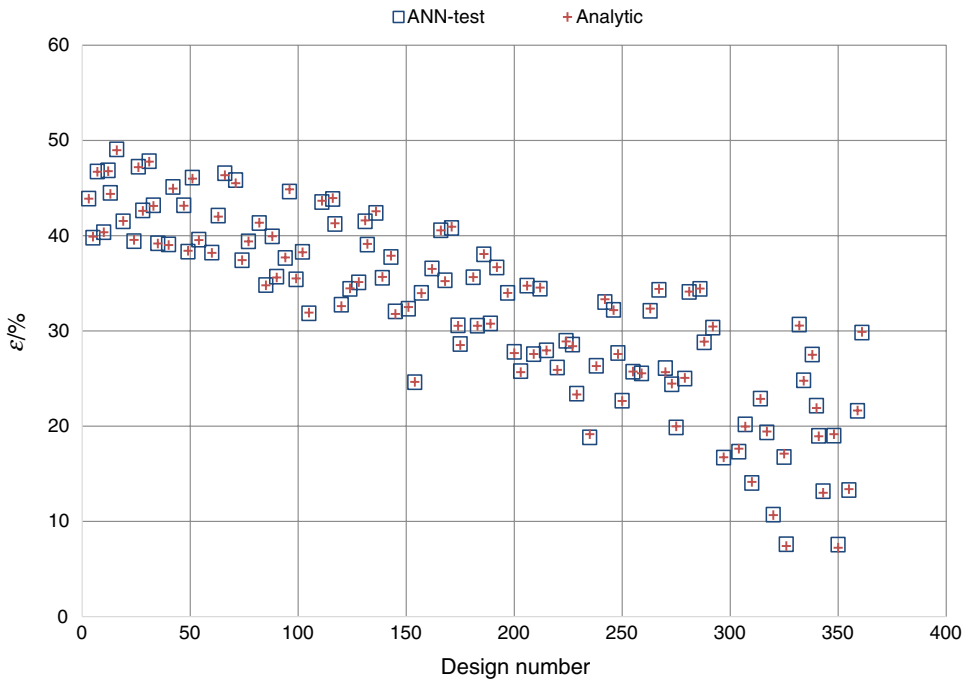

Fig. 7 Testing and analytic results of exergy efficiency

As seen in Figs. 6 and 7, the analytical and LM 2-12 ANN model results of exergy efficiency well coincided with each other. The MPE, cov, RMSE and R^2 values of training results of exergy efficiency were determined as, respectively, 0.229608, 0.40041, 0.130384 and 0.999814 for LM 2-12. These values were obtained as 0.229608, 0.400410, 0.130384 and 0.999814, respectively, for LM 2-12 in the testing step.

The power output of the turbine, the power input of the pump, the heat capacity of the evaporator, the heat capacity of the condenser and the heat capacity of the recuperator were the output parameters of the first network of the second stage. The statistical results of the first network of the second stage are given in Tables 6–10.

According to Table 6, cov, MPE, RMSE and R^2 values of training results for $\dot{W}_{tr}$ change between 0.052832–3.266416, 0.048251–3.006904, 9.792162–605.4197 and 0.9964352–0.999993, respectively. The cov, MPE, RMSE and R^2 values of testing results for $\dot{W}_{tr}$ change between 0.063841–3.5082218, 0.060240–3.628988, 12.025050–660.8064 and 0.961254–0.999990, respectively. The results obtained from Table 6 show the optimum neuron value of the hidden layer as 28 based on the percentage of absolute change. The lowest values of MPE, cov, RMSE for the power output of the turbine determination were observed with the LM algorithm with 28 neurons in the hidden layer for training and testing results. The results show that the most approximate algorithm is LM with 28 neurons in the hidden layer. The MPE, cov, RMSE and R^2 values of this model were, respectively, determined as 0.048251, 0.052832, 9.792162 and 0.999993 for training results. These values were obtained as 0.060240, 0.063841, 12.02505 and 0.999990, respectively, in the testing step.

According to Table 7, cov, MPE, RMSE and R^2 values of training results for $\dot{W}_p$ change between 0.248866–2.485783, 0.116662–1.338777, 2.908277–29.049210 and 0.995921–0.999945, respectively. The cov, MPE, RMSE and R^2 values of testing results for $\dot{W}_p$ change between 0.756402–2.706587, 0.28977–1.463305, 8.889487–31.80871 and 0.992982–0.999445, respectively. The statistical results of training values for LM 2-30 are better than LM 2-29. However, when the test values are considered, LM 2-29 has a more suitable network structure than LM 2-30. The results show that the most approximate

Table 6 The statistical results of the power output of the turbine ($\dot{W}_{tr}$)

Parameter	Algorithm	Train				Test			
		cov	MPE	RMSE	R^2	cov	MPE	RMSE	R^2
$\dot{W}_{tr}$	LM 2-4	1.165216	1.007887	215.969	0.995456	1.289192	1.270057	242.8316	0.994804
	LM 2-6	0.515148	0.41967	95.48106	0.999112	0.501062	0.47037	94.37978	0.999233
	LM 2-8	0.470425	0.399451	87.19178	0.999487	0.386907	0.390873	72.87767	0.99967
	LM 2-10	0.190662	0.174758	35.33865	0.999888	0.23218	0.207563	43.73323	0.999844
	LM 2-12	0.156152	0.130748	28.94223	0.999919	0.16052	0.149361	30.23547	0.99992
	LM 2-14	0.134418	0.108069	24.91391	0.99994	0.157179	0.140709	29.60617	0.999923
	LM 2-15	0.121175	0.103869	22.45933	0.999951	0.131965	0.119686	24.8568	0.999945
	LM 2-16	0.24651	0.211971	45.68989	0.999797	0.276687	0.271564	52.11659	0.999761
	LM 2-18	0.099214	0.086932	18.38901	0.999968	0.112487	0.111771	21.18808	0.999962
	LM 2-20	0.103114	0.094175	19.11181	0.999968	0.122909	0.114288	23.15112	0.999954
	LM 2-22	0.088324	0.076916	16.37059	0.999975	0.093803	0.083756	17.66875	0.999974
	LM 2-24	0.090184	0.078791	16.71532	0.999973	0.102906	0.094333	19.38335	0.999967
	LM 2-26	0.075255	0.064028	13.94833	0.999982	0.094772	0.089764	17.85126	0.999972
	LM 2-27	0.067164	0.059254	12.44863	0.999985	0.077051	0.077951	14.5132	0.999982
	LM 2-28	0.052832	0.048251	9.792162	0.999993	0.063841	0.060240	12.02505	0.999990
	LM 2-29	0.072574	0.064383	13.45142	0.999983	0.094937	0.089291	17.88235	0.999972
	LM 2-30	0.055222	0.050037	10.23526	0.99999	0.073281	0.068866	13.80321	0.999983
	CGP 2-4	2.961477	2.6975	548.9002	0.970648	3.235728	3.206942	609.4802	0.967023
	CGP 2-6	2.93845	2.67419	544.6322	0.971105	3.25156	3.223124	612.4624	0.966701
	CGP 2-7	1.706345	1.535752	316.2655	0.990258	1.864342	1.760277	351.1667	0.989064
	CGP 2-8	1.952568	1.710221	361.9021	0.987249	2.341014	2.176168	440.9524	0.982964
	SCG 2-4	3.035289	2.702031	562.5811	0.969185	3.261957	3.253374	614.4207	0.966527
	SCG 2-6	3.266416	3.006904	605.4197	0.964352	3.508218	3.628988	660.8064	0.961254
	SCG 2-8	1.859088	1.701294	344.576	0.988434	2.23786	2.159847	421.5223	0.984228
	SCG 2-9	2.481416	2.279484	459.9224	0.979397	2.860871	2.768053	538.8724	0.974479

Table 7 The statistical results of the power input of the pump ($\dot{W}_p$)

Parameter	Algorithm	Train				Test			
		cov	MPE	RMSE	R^2	cov	MPE	RMSE	R^2
$\dot{W}_p$	LM 2-4	1.786574	0.98607	20.87815	0.997137	1.948952	1.062038	22.90472	0.996252
	LM 2-6	1.050927	0.538795	12.28128	0.999009	1.348812	0.656614	15.85169	0.998203
	LM 2-8	0.83558	0.3997	9.764707	0.999376	1.013181	0.448285	11.90724	0.999004
	LM 2-10	0.675703	0.30001	7.896357	0.999591	0.918514	0.375927	10.79468	0.999195
	LM 2-12	0.648039	0.286533	7.57307	0.999656	0.898255	0.378054	10.55659	0.999239
	LM 2-14	0.750742	0.400136	8.773277	0.999658	0.966705	0.431754	11.36103	0.999323
	LM 2-15	0.5779	0.221709	6.753414	0.999701	0.846338	0.286178	9.946438	0.999323
	LM 2-16	0.641855	0.282831	7.50081	0.999631	0.939504	0.375759	11.04136	0.999157
	LM 2-18	0.564303	0.229935	6.594524	0.999717	0.86382	0.313066	10.1519	0.999281
	LM 2-20	0.57293	0.226231	6.695336	0.999706	0.872549	0.300211	10.25448	0.999281
	LM 2-22	0.412912	0.183461	4.825345	0.999848	0.941075	0.373208	11.05982	0.999145
	LM 2-24	0.406574	0.19165	4.751276	0.999864	0.970684	0.37607	11.4078	0.999175
	LM 2-26	0.337921	0.165524	3.94899	0.999898	0.779887	0.318081	9.165495	0.999457
	LM 2-27	0.358158	0.169312	4.185487	0.999885	0.863751	0.363306	10.15108	0.999284
	LM 2-28	0.269315	0.128243	3.147249	0.999935	0.817757	0.289770	9.610554	0.999401
	LM 2-29	0.269663	0.121057	3.151315	0.999938	0.756402	0.301510	8.889487	0.999445
	LM 2-30	0.248866	0.116662	2.908277	0.999945	0.947106	0.352995	11.13071	0.999217
	CGP 2-4	2.132771	1.118445	24.92386	0.995921	2.341596	1.292420	27.51921	0.994734
	CGP 2-6	2.140398	1.124235	25.01299	0.995892	2.314875	1.279726	27.20517	0.994898
	CGP 2-7	1.694221	0.903838	19.7989	0.997426	1.853192	1.030442	21.77933	0.996611
	CGP 2-8	1.978691	1.08003	23.12326	0.996501	2.112228	1.177519	24.8236	0.995632
	SCG 2-4	2.485783	1.338777	29.049210	0.994464	2.706587	1.463305	31.80871	0.992982
	SCG 2-6	2.040412	1.019248	23.84454	0.996274	2.183355	1.126871	25.6595	0.995419
	SCG 2-8	1.968011	1.041128	22.99846	0.996532	2.103674	1.175446	24.72306	0.995737
	SCG 2-9	1.987286	1.092519	23.2237	0.996466	2.132181	1.160790	25.0581	0.995542

algorithm is LM with 29 neurons in the hidden layer. The MPE, cov, RMSE and R^2 values of this model were, respectively, determined as 0.121057, 0.269663, 3.151315 and 0.999938 for training results. These values were obtained as 0.301510, 0.756402, 8.889487 and 0.999445, respectively, in the testing step.

According to Table 8, cov, MPE, RMSE and R^2 values of training results for $\dot{Q}_{eva}$ change between 0.001712–0.114193, 0.006204–0.429954, 2.542768–169.6526 and 0.999826–1, respectively. The cov, MPE, RMSE and R^2 values of testing results for $\dot{Q}_{eva}$ change between 0.001793–0.12304, 0.006687–0.434556, 2.679544–183.9037 and 0.999791–1, respectively. The results obtained from Table 8 show the optimum neuron value of the hidden layer as 28 based on the percentage of absolute change. The lowest values of MPE, cov, RMSE for the heat capacity of evaporator determination were observed with LM algorithm with 28 neurons in the hidden layer for training and testing results. The MPE, cov, RMSE and R^2 values of this model were, respectively, determined as 0.006204, 0.001712, 2.542768 and 1 for training results. These values were obtained as 0.006687, 0.001793, 2.679544 and 1, respectively, in the testing step.

According to Table 9, cov, MPE, RMSE and R^2 values of training results for $\dot{Q}_{con}$ change between 0.012162–0.494254, 0.037614–1.559413, 15.59851–633.9102 and 0.996920–0.999998, respectively. The cov, MPE, RMSE and R^2 values of testing results for $\dot{Q}_{con}$ change between 0.017680–0.522024, 0.040954–1.357068, 22.79025–672.9191 and 0.996441–0.999996, respectively. The results obtained from Table 9 show the optimum neuron value of the hidden layer as 28 based on the percentage of absolute change. The lowest values of MPE, cov, RMSE for the heat capacity of condenser determination were observed with LM algorithm with 28 neurons in the hidden layer for training and testing results. The MPE, cov, RMSE and R^2 values of this model were, respectively, determined as 0.037614, 0.012162, 15.59851 and 0.999998 for training results. These values were obtained as 0.040954, 0.017680, 22.79025 and 0.999996, respectively, in the testing step.

According to Table 9, cov, MPE, RMSE and R^2 values of training results for $\dot{Q}_{rec}$ change between 0.091756–6.714433, 0.040521–3.005833, 18.0078–1317.752 and 0.962766–0.999994, respectively. The cov, MPE, RMSE and R^2 values of testing results for $\dot{Q}_{rec}$ change

Table 8 The statistical results of the heat capacity of the evaporator ($\dot{Q}_{eva}$)

Parameter	Algorithm	Train				Test			
		cov	MPE	RMSE	R^2	cov	MPE	RMSE	R^2
$\dot{Q}_{eva}$	LM 2-4	0.021089	0.077524	31.3318	0.999994	0.022732	0.084055	33.97637	0.999993
	LM 2-6	0.019601	0.071314	29.12025	0.999995	0.020658	0.077011	30.87663	0.999994
	LM 2-8	0.021237	0.077494	31.55046	0.999994	0.022347	0.082851	33.40105	0.999993
	LM 2-10	0.017729	0.066324	26.33935	0.999996	0.018843	0.073144	28.16406	0.999995
	LM 2-12	0.012636	0.046518	18.77215	0.999998	0.01264	0.046933	18.89272	0.999998
	LM 2-14	0.004006	0.015146	5.951028	1	0.004136	0.015497	6.181423	1
	LM 2-15	0.007991	0.028631	11.87197	0.999999	0.008494	0.031073	12.69592	0.999999
	LM 2-16	0.020613	0.072707	30.62321	0.999994	0.021884	0.071952	32.70893	0.999993
	LM 2-18	0.002526	0.00927	3.753366	1	0.002989	0.011087	4.468178	1
	LM 2-20	0.002326	0.008256	3.455869	1	0.002425	0.008729	3.625244	1
	LM 2-22	0.00415	0.015072	6.165019	1	0.004676	0.016762	6.98963	1
	LM 2-24	0.004094	0.014166	6.081921	1	0.004052	0.015228	6.056158	1
	LM 2-26	0.003824	0.013888	5.681376	1	0.005064	0.017779	7.569107	1
	LM 2-27	0.005074	0.017531	7.538384	1	0.005874	0.020314	8.779043	1
	LM 2-28	0.001712	0.006204	2.542768	1	0.001793	0.006687	2.679544	1
	LM 2-29	0.003919	0.015025	5.822134	1	0.004327	0.016527	6.467158	1
	LM 2-30	0.003745	0.013324	5.563681	1	0.004407	0.015868	6.586469	1
	CGP 2-4	0.034554	0.133293	51.33542	0.999984	0.036017	0.139858	53.83287	0.999982
	CGP 2-6	0.030526	0.10662	45.35076	0.999987	0.030782	0.109699	46.00868	0.999987
	CGP 2-7	0.029264	0.094511	43.47564	0.999989	0.029262	0.089808	43.73707	0.999988
	CGP 2-8	0.050219	0.159405	74.60795	0.999966	0.070066	0.194495	104.7247	0.999934
	SCG 2-4	0.04692	0.178738	69.70682	0.99997	0.050742	0.194676	75.84296	0.999964
	SCG 2-6	0.051597	0.223335	76.65554	0.999997	0.053194	0.231093	79.50668	0.999996
	SCG 2-8	0.057553	0.172659	85.50439	0.999955	0.042457	0.162701	63.45923	0.999976
	SCG 2-9	0.114193	0.429954	169.6526	0.999826	0.123040	0.434556	183.9037	0.999791

between 0.121284–6.281540, 0.061052–3.303191, 23.45386–1214.724 and 0.969779–0.999990, respectively. The results obtained from Table 10 show the optimum neuron values of the hidden layer as 28 based on the percentage of absolute change. The lowest values of MPE, cov, and RMSE for the heat capacity of recuperator determination were observed with LM algorithm with 28 neurons in the hidden layer for training and testing results. The MPE, cov, RMSE and R^2 values of this model were, respectively, determined as 0.040521, 0.091756, 18.0078 and 0.999994 for training results. These values were obtained as 0.061052, 0.121284, 23.45386 and 0.999990, respectively, in the testing step.

The statistical results show that the most approximate algorithm and the number of neurons in the first network of the second stage are LM and 28, respectively, for the first network of the second-stage outputs. The investment cost (C_{ic}), the maintenance and operating costs (C_{mo}), the benefit (C_b) and the salvage cost (C_{sc}) of GEP-KC system were the output parameters of the second network of the second stage. The statistical results of the second network of the second stage are given in Tables 11–14.

According to Table 11, cov, MPE, RMSE and R^2 values of training results for C_{ic} change between 1.242421–4.249400, 1.053282–3.864230, 584526.6–1999232 and 0.939585–0.994868, respectively. The cov, MPE, RMSE and R^2 values of testing results for C_{ic} change between 1.498426–4.568396, 1.34387–4.350440, 721372–2199318 and 0.937004–0.992990, respectively. The results obtained from Table 11 show the optimum neuron values of the hidden layer as 8 based on the percentage of absolute change. The lowest values of MPE, cov, RMSE for investment cost determination were observed with LM algorithm with eight neurons in the hidden layer for training and testing results. The MPE, cov, RMSE and R^2 values of this model were, respectively, determined as 1.053282, 1.242421, 584526.6 and 0.994868 for training results. These values were obtained as 0.061052, 0.121284, 23.45386 and 0.999990, respectively, in the testing step.

According to Table 12, cov, MPE, RMSE and R^2 values of training results for C_{mo} change between 1.242421–4.249174, 1.053282–3.868719, 35071.6–119947.5 and 0.939590–0.994868, respectively. The cov, MPE, RMSE and R^2 values of testing results for C_{mo} change

Table 9 The statistical results of the heat capacity of the condenser ($\dot{Q}_{con}$)

Parameter	Algorithm	Train				Test			
		cov	MPE	RMSE	R^2	cov	MPE	RMSE	R^2
$\dot{Q}_{con}$	LM 2-4	0.205672	0.626876	263.7868	0.999466	0.209895	0.557882	270.5663	0.999416
	LM 2-6	0.143508	0.400957	184.0579	0.99974	0.112674	0.301022	145.2437	0.999833
	LM 2-8	0.132725	0.367673	170.2272	0.999798	0.113723	0.297867	146.5955	0.999862
	LM 2-10	0.085086	0.271864	109.1272	0.999909	0.091086	0.233716	117.4149	0.999891
	LM 2-12	0.054500	0.15024	69.89995	0.999963	0.053571	0.132202	69.05669	0.999962
	LM 2-14	0.046208	0.138303	59.26454	0.999973	0.049085	0.116663	63.27395	0.999968
	LM 2-15	0.040900	0.128908	52.45705	0.99998	0.039331	0.103185	50.70041	0.99998
	LM 2-16	0.059816	0.195567	76.71739	0.999955	0.061059	0.160179	78.70904	0.999952
	LM 2-18	0.024466	0.078343	31.37959	0.999992	0.030047	0.079935	38.73242	0.999989
	LM 2-20	0.031249	0.094009	40.0784	0.999988	0.038559	0.086616	49.70511	0.999981
	LM 2-22	0.034041	0.102026	43.66004	0.999986	0.040493	0.103077	52.19806	0.999979
	LM 2-24	0.023506	0.072744	30.1483	0.999993	0.033442	0.086773	43.10812	0.999985
	LM 2-26	0.021205	0.06498	27.19667	0.999994	0.024466	0.062141	31.53829	0.999993
	LM 2-27	0.018095	0.055002	23.20827	0.999996	0.024365	0.060924	31.40768	0.999992
	LM 2-28	0.012162	0.037614	15.59851	0.999998	0.017680	0.040954	22.79025	0.999996
	LM 2-29	0.024272	0.074011	31.13007	0.999993	0.027902	0.067186	35.96768	0.99999
	LM 2-30	0.014973	0.04657	19.20399	0.999997	0.022684	0.053693	29.24096	0.999993
	CGP 2-4	0.492541	1.559413	631.7128	0.996938	0.519887	1.320346	670.1644	0.996469
	CGP 2-6	0.474534	1.514136	608.6175	0.997158	0.50953	1.297734	656.8129	0.996603
	CGP 2-7	0.252346	0.763099	323.6488	0.999197	0.267198	0.661936	344.433	0.999059
	CGP 2-8	0.324496	1.02201	416.1853	0.998679	0.370827	0.935834	478.0173	0.998185
	SCG 2-4	0.491262	1.53338	630.0721	0.996954	0.519231	1.339268	669.3184	0.996468
	SCG 2-6	0.494254	1.556856	633.9102	0.996920	0.522024	1.357068	672.9191	0.996441
	SCG 2-8	0.320582	0.999755	411.1652	0.998703	0.363119	0.955705	468.0807	0.998284
	SCG 2-9	0.433929	1.334208	556.539	0.997624	0.489793	1.214753	631.3703	0.996828

between 1.498426–4.532546, 1.343870–4.322735, 43282.35–130923.6 and 0.938090–0.992990, respectively. The results obtained from Table 12 show the optimum neuron values of the hidden layer as 8 based on the percentage of absolute change. The lowest values of MPE, cov, RMSE for maintenance and operating costs determination were observed with LM algorithm with eight neurons in the hidden layer for training and testing results. The MPE, cov, RMSE and R^2 values of this model were, respectively, determined as 1.053282, 1.242421, 35071.6 and 0.994868 for training results. These values were obtained as 1.343870, 1.498426, 43282.35 and 0.992990, respectively, in the testing step.

According to Table 13, cov, MPE, RMSE and R^2 values of training results for C_b change between 0.267812–2.658207, 0.188479–2.039295, 23923.89–237460.4 and 0.980082–0.999798, respectively. The cov, MPE, RMSE and R^2 values of testing results for C_b change between 0.285935–2.611736, 0.232122–2.293514, 25976.47–237269.5 and 0.982064–0.999784, respectively. The results obtained from Table 13 show the optimum neuron values of the hidden layer as 7 based on the percentage of absolute change. The lowest values of MPE, cov, RMSE for benefit determination were observed with LM algorithm with seven neurons in the hidden layer for training and testing results. The MPE, cov, RMSE and R^2 values of this model were, respectively, determined as 0.188479, 0.267812, 23923.89 and 0.999798 for training results. These values were obtained as 0.232122, 0.285935, 25976.47 and 0.999784, respectively, in the testing step.

According to Table 14, cov, MPE, RMSE and R^2 values of training results for C_{sc} change between 1.242421–4.249496, 1.310181–4.815029, 58452.66–199927.7 and 0.939580–0.994868, respectively. The cov, MPE, RMSE and R^2 values of testing results for C_{sc} change between 1.498426–4.56964, 1.343870–4.355962, 72137.25–219991.7 and 0.937210–0.992990, respectively. The results show that the most approximate algorithm is LM with eight neurons in the hidden layer. The MPE, cov, RMSE and R^2 values of this model were, respectively, determined as 1.310181, 1.242421, 58452.66 and 0.994868 for training results. These values were obtained as 1.343870, 1.498426, 72137.25 and 0.992990, respectively in the testing step.

Table 10 The statistical results of the heat capacity of the recuperator ($\dot{Q}_{rec}$)

Parameter	Algorithm	Train				Test			
		cov	MPE	RMSE	R^2	cov	MPE	RMSE	R^2
$\dot{Q}_{rec}$	LM 2-4	4.04815	1.378359	794.4761	0.986384	2.728114	1.493559	527.5624	0.994187
	LM 2-6	2.748721	0.617065	539.4546	0.993722	1.452571	0.625674	280.8981	0.998463
	LM 2-8	2.738185	0.784782	537.3869	0.994425	1.66731	0.771751	322.4243	0.998325
	LM 2-10	0.386044	0.177578	75.76361	0.999877	0.403499	0.209806	78.02867	0.999877
	LM 2-12	0.287346	0.128741	56.39358	0.999935	0.332794	0.166895	64.35575	0.999919
	LM 2-14	0.248528	0.102467	48.77527	0.999952	0.300987	0.153563	58.20489	0.999931
	LM 2-15	0.235139	0.103518	46.1475	0.999954	0.261827	0.138115	50.63217	0.999946
	LM 2-16	0.417339	0.17482	81.9055	0.999856	0.415174	0.210201	80.28637	0.999867
	LM 2-18	0.190928	0.085698	37.47089	0.999974	0.230338	0.117105	44.54281	0.999964
	LM 2-20	0.186803	0.079842	36.66127	0.999971	0.225257	0.112723	43.56027	0.999961
	LM 2-22	0.164374	0.07363	32.25957	0.999978	0.252903	0.122104	48.90627	0.99995
	LM 2-24	0.185381	0.078596	36.38229	0.999971	0.250617	0.12263	48.46438	0.99995
	LM 2-26	0.111625	0.049302	21.90721	0.99999	0.133374	0.069407	25.79184	0.999987
	LM 2-27	0.140104	0.062141	27.49624	0.999986	0.18307	0.093535	35.40212	0.999976
	LM 2-28	0.091756	0.040521	18.0078	0.999994	0.121284	0.061052	23.45386	0.999990
	LM 2-29	0.107888	0.047271	21.17377	0.99999	0.166678	0.075297	32.23219	0.999978
	LM 2-30	0.111188	0.047088	21.82135	0.99999	0.170321	0.083896	32.93659	0.999977
	CGP 2-4	5.053655	2.082797	991.8131	0.978781	4.370031	2.37796	845.0763	0.985023
	CGP 2-6	5.179081	2.13265	1016.429	0.977714	4.619793	2.509185	893.3752	0.983196
	CGP 2-7	4.267502	1.496676	837.5255	0.98487	3.460071	1.840121	669.1083	0.990605
	CGP 2-8	4.668862	1.749375	916.295	0.981891	4.055245	2.128752	784.2029	0.987039
	SCG 2-4	5.385799	2.202867	1056.999	0.975922	5.046286	2.65788	975.8504	0.979973
	SCG 2-6	6.714433	3.005833	1317.752	0.962766	6.281540	3.303191	1214.724	0.969779
	SCG 2-8	4.241705	1.513847	832.4626	0.985051	3.438131	1.835352	664.8654	0.990749
	SCG 2-9	4.885669	1.86868	958.8448	0.980173	4.30659	2.140341	832.8079	0.985389

Table 11 The statistical results of the investment cost (C_{ic})

Parameter	Algorithm	Train				Test			
		cov	MPE	RMSE	R^2	cov	MPE	RMSE	R^2
C_{ic}	LM 2-4	2.503619	2.315552	1177887	0.979319	2.716881	2.473808	1307962	0.979535
	LM 2-6	1.602719	1.280404	754037.2	0.991471	1.765581	1.502209	849986	0.990979
	LM 2-7	1.382848	1.230163	650593.6	0.993629	1.802712	1.682278	867862	0.990307
	LM 2-8	1.242421	1.053282	584526.6	0.994868	1.498426	1.343870	721372	0.992990
	LM 2-9	1.288588	1.129656	606247.1	0.995290	2.105272	1.76756	1013521	0.989238
	CGP 2-4	4.249400	3.864230	1999232	0.939585	4.255438	3.988129	2048654	0.944573
	CGP 2-6	4.161557	3.777248	1957904	0.942057	4.368873	4.152793	2103264	0.941495
	CGP 2-8	3.268519	3.022987	1537752	0.964331	3.520464	3.383677	1694823	0.962517
	CGP 2-9	3.441421	3.129785	1619098	0.960373	3.996079	3.615777	1923793	0.951511
	CGP 2-10	3.651632	3.336107	1717997	0.955387	3.860695	3.625075	1858617	0.953955
	SCG 2-4	4.18205	3.771625	1967545	0.941512	4.182714	3.900043	2013643	0.946241
	SCG 2-6	3.998116	3.70161	1881009	0.946651	4.180133	4.004597	2012401	0.946024
	SCG 2-8	4.193615	3.624144	1972986	0.941167	4.362006	4.056487	2099958	0.941985
	SCG 2-10	3.824512	3.550591	1799333	0.951063	4.568396	4.350440	2199318	0.937004
	SCG 2-12	2.904512	2.685216	1366497	0.971775	2.976861	2.886317	1433121	0.973564
	SCG 2-13	2.940810	2.815018	1383574	0.971066	3.133334	2.920143	1508450	0.969974
	SCG 2-14	3.650784	3.364428	1717598	0.955411	4.059784	3.829858	1954462	0.949314

Table 12 The statistical results of the maintenance and operating costs (C_{mo})

Parameter	Algorithm	Train				Test			
		cov	MPE	RMSE	R^2	cov	MPE	RMSE	R^2
C_{mo}	LM 2-4	2.503619	2.315552	70673.24	0.979319	2.716881	2.473808	78477.71	0.979535
	LM 2-6	1.602719	1.280404	45242.23	0.991471	1.765581	1.502209	50999.19	0.990979
	LM 2-7	1.382848	1.230163	39035.62	0.993629	1.802712	1.682278	52071.73	0.990307
	LM 2-8	1.242421	1.053282	35071.6	0.994868	1.498426	1.343870	43282.35	0.992990
	LM 2-9	1.282726	1.123098	36209.34	0.995290	2.098058	1.759158	60602.87	0.989238
	CGP 2-4	4.249174	3.868719	119947.5	0.939590	4.255502	3.992831	122921.1	0.944543
	CGP 2-6	4.162811	3.768353	117509.6	0.942021	4.36624	4.146048	126119.8	0.941634
	CGP 2-8	3.268968	3.011051	92277.84	0.964245	3.519847	3.371914	101671.5	0.962202
	CGP 2-9	3.445335	3.124396	97256.41	0.960395	4.046204	3.669505	116875.5	0.950360
	CGP 2-10	3.650523	3.330951	103048.5	0.955415	3.857934	3.620769	111437.3	0.954027
	SCG 2-4	4.170625	3.798113	117730.2	0.941802	4.176432	3.931571	120637.2	0.946388
	SCG 2-6	3.992876	3.740699	112712.6	0.946673	4.178143	4.089758	120686.6	0.946119
	SCG 2-8	4.190161	3.616413	118281.7	0.941256	4.365432	4.053156	126096.5	0.941800
	SCG 2-10	3.824994	3.550725	107973.6	0.951051	4.532546	4.322735	130923.6	0.938090
	SCG 2-12	2.901328	2.688084	81899.93	0.971836	2.968252	2.88646	85738.59	0.973716
	SCG 2-13	2.950019	2.816512	83274.4	0.970887	3.143501	2.893179	90800.7	0.969838
	SCG 2-14	3.63695	3.345654	102665.4	0.955746	4.119736	3.857322	118999.5	0.947714

Table 13 The statistical results of the benefit (C_b)

Parameter	Algorithm	Train				Test			
		cov	MPE	RMSE	R^2	cov	MPE	RMSE	R^2
C_b	LM 2-4	0.43256	0.337038	38641.02	0.999552	0.419378	0.355453	38099.44	0.99958
	LM 2-6	0.287979	0.198492	25725.49	0.999771	0.294596	0.239886	26763.34	0.999781
	LM 2-7	0.267812	0.188479	23923.89	0.999798	0.285935	0.232122	25976.47	0.999784
	LM 2-8	0.319645	0.251826	28554.19	0.999712	0.304506	0.255067	27663.61	0.999754
	LM 2-9	0.649858	0.465527	58052.53	0.998809	0.637065	0.50441	57875.72	0.998931
	CGP 2-4	2.520659	1.963000	225173.1	0.982079	2.486306	2.191779	225874.5	0.983731
	CGP 2-6	1.437851	1.103574	128444.8	0.994192	1.590916	1.356552	144530.7	0.993293
	CGP 2-8	1.364048	1.061055	121851.8	0.994771	1.433223	1.195017	130204.6	0.99455
	CGP 2-9	1.625698	1.304252	145225.3	0.992545	1.512581	1.344281	137414.1	0.993955
	CGP 2-10	2.197967	1.609955	196346.6	0.986375	1.94066	1.658727	176304	0.990037
	SCG 2-4	2.658207	2.039295	237460.4	0.980082	2.611736	2.293514	237269.5	0.982064
	SCG 2-6	2.476429	1.920139	221221.9	0.982765	2.530126	2.110123	229855.5	0.983426
	SCG 2-8	2.370338	1.899965	211744.8	0.984159	2.484392	2.183866	225700.7	0.983695
	SCG 2-10	1.891059	1.564753	168930.3	0.989915	1.994526	1.75222	181197.6	0.989503
	SCG 2-12	1.447462	1.118705	129303.3	0.994106	1.462627	1.243832	132875.9	0.994704
	SCG 2-13	1.565677	1.285133	139863.6	0.993086	1.530978	1.326436	139085.4	0.993784
	SCG 2-14	1.482011	1.192767	132389.6	0.993806	1.610521	1.396199	146311.7	0.99314

The statistical results show that the most approximate algorithm and the number of neurons in the second network of the second stage are LM and 8, respectively. The NVP was the output of the third network in the second stage of the proposed multi-stage ANN model. The statistical result of NPV is given in Table 15.

According to Table 15, cov, MPE, RMSE and R^2 values of training results for NPV change between 0.013915–1.806788, 0.006398–0.858056, 0.009669–1.255459 and 0.997352–1, respectively. The cov, MPE, RMSE and R^2 values of testing results for NPV change between 0.015455–2.016340, 0.007532–1.016980, 0.010830–1.412925 and 0.997088–1,

Table 14 The statistical results of the salvage cost (C_{sc})

Parameter	Algorithm	Train				Test			
		cov	MPE	RMSE	R^2	cov	MPE	RMSE	R^2
C_{sc}	LM 2-4	2.503619	2.880321	117788.7	0.979319	2.716881	2.473808	130796.2	0.979535
	LM 2-6	1.602719	1.592698	75403.72	0.991471	1.765581	1.502209	84998.65	0.990979
	LM 2-7	1.382848	1.530203	65059.36	0.993629	1.802712	1.682278	86786.22	0.990307
	LM 2-8	1.242421	1.310181	58452.66	0.994868	1.498426	1.343870	72137.25	0.992990
	LM 2-9	1.273311	1.384345	59905.94	0.995289	2.086223	1.745275	100435	0.989238
	CGP 2-4	4.249496	4.815029	199927.7	0.939580	4.256473	3.995929	204915.2	0.944516
	CGP 2-6	4.165878	4.705376	195993.7	0.942013	4.335392	4.101225	208714.6	0.94176
	CGP 2-8	3.272577	3.751051	153966.2	0.964167	3.530698	3.378122	169975	0.961953
	CGP 2-9	3.441735	3.876212	161924.6	0.960385	4.004547	3.626029	192787	0.951397
	CGP 2-10	3.651569	4.142959	171796.8	0.955388	3.853177	3.613854	185499.8	0.9541
	SCG 2-4	4.191132	4.776435	197181.8	0.941244	4.208095	3.997632	202586.2	0.945563
	SCG 2-6	4.024901	4.646718	189361.1	0.945815	4.145015	4.030108	199549.4	0.946963
	SCG 2-8	4.187116	4.502601	196992.8	0.941346	4.35616	4.050476	209714.4	0.942111
	SCG 2-10	3.822668	4.392191	179846.5	0.951113	4.56964	4.355962	219991.7	0.937210
	SCG 2-12	2.900072	3.348387	136440.8	0.971865	3.006869	2.927842	144756.8	0.973037
	SCG 2-13	3.00027	3.592388	141154.9	0.969886	3.233226	3.069008	155654.1	0.968009
	SCG 2-14	3.653738	4.194032	171898.8	0.955339	4.056538	3.837675	195290	0.949349

Table 15 The statistical results of NPV

Parameter	Algorithm	Train				Test			
		cov	MPE	RMSE	R^2	cov	MPE	RMSE	R^2
NPV	LM 2-4	0.013915	0.006398	0.009669	1	0.015455	0.007532	0.010830	1
	LM 2-5	0.068284	0.041865	0.047447	1	0.068238	0.045267	0.047817	1
	LM 2-6	0.03065	0.017407	0.021297	1	0.033086	0.019638	0.023185	1
	CGP 2-4	1.282924	0.597296	0.891449	0.998665	1.387508	0.671421	0.972279	0.998646
	CGP 2-5	0.410188	0.143290	0.285022	0.999864	0.476046	0.168500	0.333583	0.999835
	CGP 2-6	1.806788	0.858056	1.255459	0.997352	2.016340	1.016980	1.412925	0.997088
	SCG 2-4	0.644212	0.307057	0.447635	0.999663	0.845596	0.371846	0.592541	0.999482
	SCG 2-6	0.662124	0.317478	0.460082	0.999644	0.961239	0.417611	0.673576	0.999329
	SCG 2-8	0.745911	0.309341	0.518302	0.999548	0.804624	0.348188	0.563831	0.999532

respectively. The results obtained from Table 15 show the optimum neuron value of the hidden layer as 4 based on the percentage of absolute change. The lowest values of MPE, cov, and RMSE for benefit determination were observed with LM algorithm with four neurons in the hidden layer for training and testing results. The NPV results are given in Figs. 8 and 9 for training and test values for LM 2-4.

As seen in Figs. 8 and 9, the analytical and LM 2-4 ANN model results of NPV well coincided with each other. The results show that the most approximate algorithm is LM with four neurons in the hidden layer. The MPE, cov, RMSE and R^2 values of this model were, respectively, determined as 0.006398, 0.013915, 0.009669 and 1 for training results. These values were obtained as 0.007532, 0.015455, 0.010830 and 1, respectively, in the testing step.

The R^2 values of the whole multi-stage ANN model networks changed between 0.994868 and 1. These values are the acceptable range for the ANN optimization of energy systems. The cov, MPE, RMSE and R^2 values of NPV were determined, respectively, as 2.558308, 1.077997189, 1.777658128 and 0.994693 for training results of the multi-stage ANN model. These values were obtained as 3.113911, 1.466969, 2.182035 and 0.993136, respectively, in the testing step.

The optimum GEP-KC system parameters were determined by maximizing the NPV value of the GEP-KC by using the masses and biases of the best algorithms of each network. The optimum parameters of GEP-KC were determined as P_4= 5000 kPa, P_7= 820 kPa, T_{2b}= 353.15 K and α = 90% according to the multi-stage ANN network. Also,

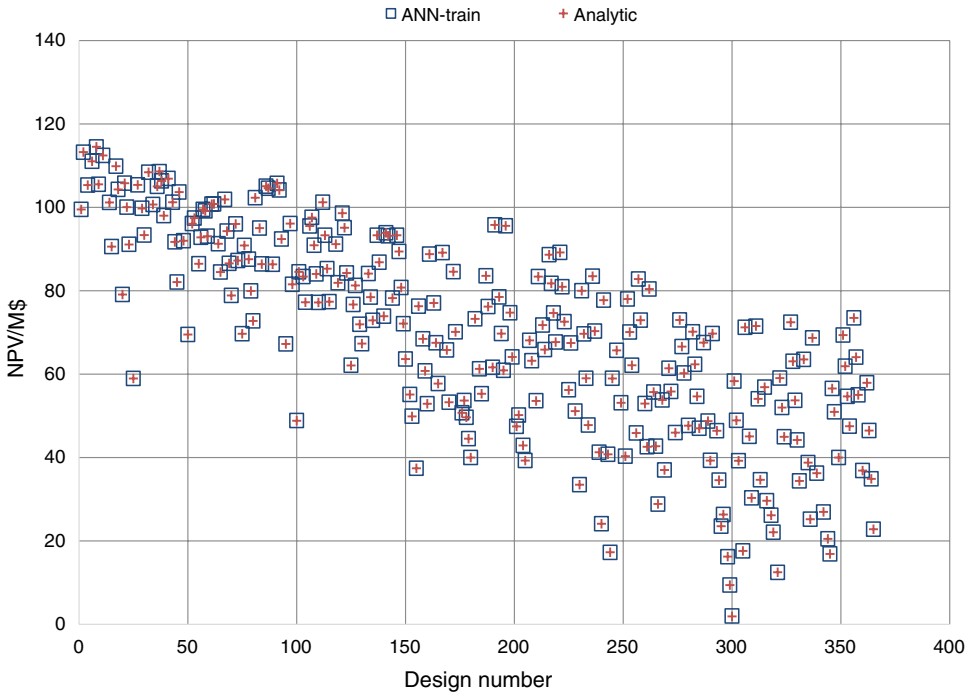

Fig. 8 Training and analytic results of NPV

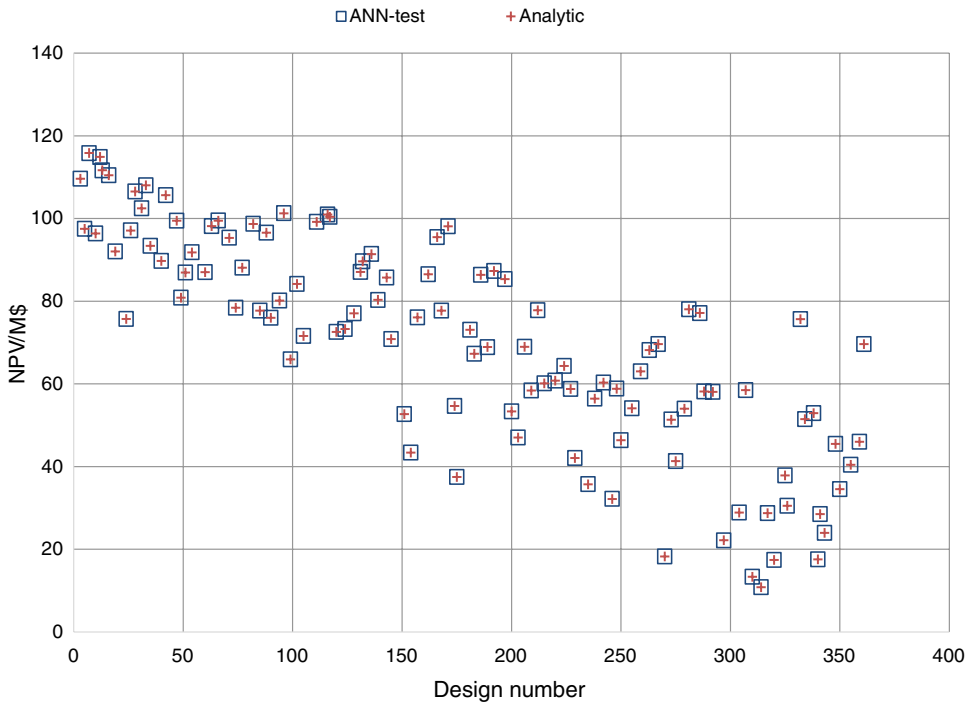

Fig. 9 Testing and analytic results of NPV

energy, exergy and economic analysis were made for optimum design parameters. The thermodynamic properties of the optimum GEP-KC are given in Table 16. The ANN and analytical results are given in Table 17 for optimum GEP-KC.

According to the results in Table 17, the analytical results well coincided with the ANN results. The minimum error rate was determined for evaporator as 0.000432%, and the maximum error rate was calculated for investment cost, maintenance and operating costs and salvage cost as 3.014745%. The NPV was calculated as 113.0732 M$ analytically for optimum GEP-KC, and the error rate was determined as 0.938314%. The error rates of energy

Table 16 The thermodynamic properties of the optimum GEP-KC

Point	T/K	P/kPa	h/kJ kg^{-1}	s/kJ kg^{-1} K^{-1}	$\dot{m}$ /kg s^{-1}	α/%	Ψ_{ch}/kJ kg^{-1}	Ψ_{ph}/kJ kg^{-1}
1	295.06	820	333.500	1.6387	149.2705	90	17863.52	185.9548
2	296.22	5000	341.475	1.6441	149.2706	90	17863.51	192.3198
3	315.26	5000	432.730	1.9426	149.2706	90	17863.51	194.5770
4	398.15	5000	1537.200	4.9460	149.2706	90	17863.51	403.5833
5	398.15	5000	1776.900	5.5662	119.2976	0.96705	19190.61	458.3707
6	398.15	5000	583.290	2.4775	29.9730	0.64119	12581.42	127.7375
7	313.56	820	1562.275	5.6880	119.2976	0.96705	19190.61	207.4310
8	326.34	820	583.290	2.6259	29.97304	0.64119	12581.40	141.4111
9	320.26	820	1365.698	5.0749	149.2706	90	17863.51	193.6498
10	310.34	820	1258.339	4.7339	149.2706	90	17863.51	187.9602
2a	406.65	300	777.130	2.2030	462.0000	–		461.3300
2b	353.15	300	335.210	1.0754	462.0000	–		355.6100
3a	288.15	4	62.984	0.2244	3299.0300	–		728.5923
3b	298.15	4	104.830	0.3672	3450.3130	–		727.8744

Table 17 The ANN and analytical results of optimum GEP-KC

Parameter	ANN	Analytic	Error rate/%
$\dot{W}_{tr}$/W	25407984	25604237	0.766485
$\dot{W}_{p}$/W	1208332	1190433	1.503566
$\dot{Q}_{eva}$/W	164865597	164864884	0.000432
$\dot{Q}_{con}$ (W)	138557404	138051298	0.366608
$\dot{Q}_{rec}$ (W)	13894557	13621687	2.003207
η (%)	6.650826	6.728543	1.155038
ε (%)	46.36653	46.87011	1.07442
C_{ic}(M$)	56.69869	58.46114	3.014745
C_{mo}(M$)	3.401921	3.507668	3.014745
C_{b}(M$)	12.42832	12.56081	1.054805
C_{sc}(M$)	5.669869	5.846114	3.014745
NPV$(M\$)$	114.1342	113.0732	0.938314

efficiency and exergy efficiency were calculated as 1.155038 and 1.07442, respectively.

This analysis was also performed for the single network ANN model for the determination of NPV, energy efficiency and exergy efficiency by using the first network inputs. However, the results of the multi-stage ANN model were found to be more consistent than the single network model. In addition, it was determined in nine different parameters which should be considered in the evaluation of the GEP-KC in the multi-stage ANN model.

Conclusions

The GEP-KC was designed for different turbine inlet pressure ($P_4 = P_5$), the geothermal water outlet temperature at the evaporator (T_{2b}), condenser pressure ($P_7 = P_{10}$) and ammonia mass fraction (α). Also, NPV, energy and exergy values of these models were determined analytically. Analytical results of 365 GEP-KC designs were used in ANN analysis. Moreover, 70% of the designed models were used for training and 30% of the designed models were used for testing. The ANN model was basically composed of two stages. The first has a single network, and the second stage consists of three networks in this ANN model. Turbine inlet pressure, the geothermal water outlet temperature at the evaporator, condenser pressure and ammonia mass fraction were input parameters of the multi-stage ANN model. Energy and exergy efficiencies of the GEP-KC were the output parameters of the first stage. The NPV was the output parameter of the second stage consisting of three networks. The optimum GEP-KC system parameters were determined by maximizing the NPV value of the GEP-KC by using the masses and biases of the best algorithms of each network. The performance of ANN was determined by using different statistical methods such as cov, MPE, RMSE and R^2. These statistical values were used to determine the best algorithm for the multi-stage ANN model and to evaluate the precision and usability of the multi-stage ANN model for system optimization. The statistical results showed that LM was the best suitable algorithm for all ANN stages. The statistical results showed that the optimum neuron values of hidden layers in the first network, second network and third network of second stage were determined as 28, 8 and 4, respectively.

Optimum system parameters are determined as $P_4 = 5000$ kPa, $P_7 = 820$ kPa, $T_{2b} = 353.15$ K and $\alpha = 90\%$ according to the multi-stage ANN network. The cov, MPE, RMSE and R^2 values of NPV were determined, respectively, as 2.558308, 1.077997189, 1.777658128 and 0.994693 for the multi-stage ANN model in the training step. These values are within acceptable limits from a statistical point of

view. According to the statistical results, ANN results of the outputs well coincided with the analytical results. The minimum error rate was determined for evaporator as 0.000432% and the maximum error rates were calculated for investment cost, maintenance and operating costs and salvage cost as 3.014745% for analytical and statistical analysis results of optimum GEP-KC. The energy and exergy efficiencies of the optimum GEP-KC model were determined, respectively, as 6.6508% and 46.3665% in the multi-stage ANN network. These values were analytically determined as 6.7285% and 46.8701%, respectively. The NPV was calculated as 113.0732 M$ analytically and 114.1341 M$ statistically for optimum GEP-KC, and the error rate was determined as 0.938314%. It is seen that there is good conformity between the analytical and ANN results. According to the analytical and statistical results, the multi-stage ANN model is very sufficient for the optimization of GEP-KC. The error rates in the pre-decision stage of the system design are appropriate in terms of engineering. As a result, this study shows that the multi-stage ANN model could be used for the design and optimization of different energy systems with high accuracy.

Funding Not applicable.

Data availability All data generated or analyzed during this study are included in this article.

Compliance with ethical standards

Conflict of interest The authors declare that they have no conflict of interest.

Ethics approval and consent to participate Not applicable.

References

1. Rodríguez CEC, Palacio JCE, Venturini OJ, Lora EES, Cobas VM, dos Santos DM, Dotto FRL, Gialluca V. Exergetic and economic comparison of ORC and Kalina cycle for low temperature enhanced geothermal system in Brazil. Appl Therm Eng. 2013;52(1):109–19.
2. Cao L, Wang J, Chen L, Dai Y. Comprehensive analysis and optimization of Kalina–flash cycles for low-grade heat source. Appl Therm Eng. 2018;131:540–52.
3. Ashouri M, Vandani AMK, Mehrpooya M, Ahmadi MH, Abdollahpour A. Techno-economic assessment of Kalina cycle driven by a parabolic trough solar collector. Energy Convers Manag. 2015;105:1328–39.
4. Reddy KS, Ananthsornaraj C. Design, development and performance investigation of solar parabolic trough collector for large-scale solar power plants. Renew Energy. 2020;146:1943–57.
5. Acar MS, Arslan O. Energy and exergy analysis of solar energy-integrated, geothermal energy-powered organic Rankine cycle. J Therm Anal Calorim. 2019;137(2):659–66.
6. Arslan O. Exergoeconomic evaluation of electricity generation by the medium temperature geothermal resources, using a Kalina cycle: Simav case study. Int J Therm Sci. 2010;49(9):1866–73.
7. Ahmadi MH, Mehrpooya M, Pourfayaz F. Exergoeconomic analysis and multi objective optimization of performance of a carbon dioxide power cycle driven by geothermal energy with liquefied natural gas as its heat sink. Energy Convers Manag. 2016;119:422–34.
8. Ahmadi MH, Mehrpooya M, Pourfayaz F. Thermodynamic and exergy analysis and optimization of a transcritical CO_2 power cycle driven by geothermal energy with liquefied natural gas as its heat sink. Appl Therm Eng. 2016;109:640–52.
9. Sadaghiani MS, Ahmadi MH, Mehrpooya M, Pourfayaz F, Feidt M. Process development and thermodynamic analysis of a novel power generation plant driven by geothermal energy with liquefied natural gas as its heat sink. Appl Therm Eng. 2018;133:645–58.
10. Ahmadi MH, Banihashem SA, Ghazvini M, Sadeghzadeh M. Thermo-economic and exergy assessment and optimization of performance of a hydrogen production system by using geothermal energy. Energy Environ. 2018;29(8):1373–92.
11. Abdolalipouradl M, Khalilarya S, Jafarmadar S. Exergoeconomic analysis of a novel integrated transcritical CO_2 and Kalina 11 cycles from Sabalan geothermal power plant. Energy Convers Manag. 2019;195:420–35.
12. Walravena D, Laenenb B, D'haeseleer W. Comparison of thermodynamic cycles for power production from low-temperature geothermal heat sources. Energy Convers Manag. 2013;66:220–33.
13. Wang ZX, Du S, Wang LW, Chen X. Parameter analysis of an ammonia-water power cycle with a gravity assisted thermal driven "pump" for low-grade heat recovery. Renew Energy. 2020. https://doi.org/10.1016/j.renene.2019.07.014.
14. Lucia U. Exergy flows as bases of constructal law. Phys A. 2013;392(24):6284–7.
15. Lucia U. The wasted primary resource value: an indicator for the thermodynamics of sustainability for municipalities policy. Int J Thermodyn. 2017;20(3):166–72.
16. Lucia U, Grisolia G. Unavailability percentage as energy planning and economic choice parameter. Renew Sustain Energy Rev. 2017;75:197–204.
17. Lucia U, Grisolia G. Cyanobacteria and microalgae: thermoeconomic considerations in biofuel production. Energies. 2018;11:156–71.
18. Lucia U, Grisolia G. Exergy inefficiency: an indicator for sustainable development analysis. Energy Rep. 2019;5:62–9.
19. Valdimarsson P, Eliasson L. Factors influencing the economics of the Kalina power cycle and situations of superior performance. In: Proceedings of international geothermal conference 2003; Reykjavik, pp 31–9.
20. DiPippo R. Second law assessment of binary plants generating power from low-temperature geothermal fluids. Geothermics. 2004;33:565–86.
21. Nag PK, Gupta AVSSKS. Exergy analysis of the Kalina cycle. Appl Therm Eng. 1998;18:427–39.
22. Borgert JA, Velasquez JA. Exergoeconomic optimization of a Kalina cycle for power generation. Int J Exergy. 2004;1:18–28.
23. Desideri U, Bidini G. Study of possible optimization criteria for geothermal power plants. Energy Convers Manag. 1997;38:1681–91.
24. Meng F, Wang E, Zhang B, Zhang F, Zhao C. Thermo-economic analysis of transcritical CO_2 power cycle and comparison with Kalina cycle and ORC for a low-temperature heat source. Energy Convers Manag. 2019;195:1295–308.
25. Keyvani M, Afrand M, Toghraie D, Reiszadeh M. An experimental study on the thermal conductivity of cerium oxide/ethylene glycol nanofluid: developing a new correlation. J Mol Liq. 2018;266:211–7.

26. Ramezanizadeh M, Nazari MA, Ahmadi MH, Lorenzini G, Pop I. A review on the applications of intelligence methods in predicting thermal conductivity of nanofluids. J Therm Anal Calorim. 2019;138:827–43.
27. Yashawantha KM, Vinod AV. ANN modelling and experimental investigation on effective thermal conductivity of ethylene glycol:water nanofluids. J Therm Anal Calorim. 2020. https://doi.org/10.1007/s10973-020-09756-y.
28. Parashar N, Aslfattahi N, Yahya SM, Saidur R. An artificial neural network approach for the prediction of dynamic viscosity of MXene-palm oil nanofluid using experimental data. J Therm Anal Calorim. 2020. https://doi.org/10.1007/s10973-020-09638-3.
29. Barewar SD, Tawri S, Chougule S. Experimental investigation of thermal conductivity and its ANN modeling for glycol-based Ag/ZnO hybrid nanofluids with low concentration. J Therm Anal Calorim. 2020;139:1779–90.
30. Sencan A, Kalogirou SA. A new approach using artificial neural networks for determination of the thermodynamic properties of fluid couples. Energy Convers Manag. 2005;46:2405–18.
31. Sozen A, Ozalp M, Arcaklıoglu E, Kanit EG. A study for estimating solar resources in Turkey using artificial neural network. Energy Sources. 2004;26:1369–78.
32. Kalogirou SA. Artificial neural networks in renewable energy systems applications: a review. Renew Sustain Energy Rev. 2001;5:373–401.
33. Farzaneh-Gord M, Rahbari HR, Mohseni-Gharyehsafa B, Toikka A, Zvereva I. Machine learning methods for precise calculation of temperature drop during a throttling process. J Therm Anal Calorim. 2020;140:2765–78.
34. Toghyani S, Ahmadi MH, Kasaeian A, Mohammadi AH. Artificial neural network, ANN-PSO and ANN-ICA for modelling the Stirling enginet. Int J Ambien Energy. 2016;37(5):456–68.
35. Wang J, Sun Z, Dai Y, Ma S. Parametric optimization design for supercritical CO_2 power cycle using genetic algorithm and artificial neural network. Appl Energy. 2010;87:1317–24.
36. Saffari H, Sadeghi S, Khoshzat M, Mehregan P. Thermodynamic analysis and optimization of a geothermal Kalina cycle system using Artificial Bee Colony algorithm. Renew Energy. 2016;89:154–67.
37. Sadeghi S, Saffari H, Bahadormanesh N. Optimization of a modified double-turbine Kalina cycle by using Artificial Bee Colony algorithm. Appl Therm Eng. 2015;2015(91):19–32.
38. Arslan O. Power generation from medium temperature geothermal resources: ANN-based optimization of Kalina cycle system-34. Energy. 2011;36(5):2528–34.
39. Arat H, Arslan O. Optimization of district heating system aided by geothermal heat pump: a novel multistage with multilevel ANN modelling. Appl Therm Eng. 2017;111:608–23.
40. Tugcu A, Arslan O. Optimization of geothermal energy aided absorption refrigeration system- GAARS: a novel ANN-based approach. Geothermics. 2017;65:210–21.
41. Arslan O. Ultimate evaluation of Simav-Eynal geothermal resources: design of integrated system and its energy-exergy analysis. Ph.D. thesis. Eskisehir: Eskisehir Osmangazi University. Institute of Applied Sciences; 2008 (in Turkish).
42. Lemmon EW, Bell IH, Huber ML, McLinden MO. NIST Standard Reference Database 23: Reference Fluid Thermodynamic and Transport Properties-REFPROP. Version 10.0, National Institute of Standards and Technology USA; 2019.
43. Bejan A, Tsatsaronis G, Moran M. Thermal design and optimization. New York: Wiley; 1996.
44. Acar MS, Arslan O. Exergo-economic EVALUATION of a new drying system boosted by Ranque–Hilsch vortex tube. Appl Therm Eng. 2017;124:1–16.
45. Aminyavari M, Najafi B, Shirazi A, Rinaldi F. Exergetic, economic and environmental (3E) analyses, and multi objective optimization of a CO_2/NH_3 cascade refrigeration system. Appl Therm Eng. 2014;65:42–50.
46. Chemical Engineering Plant Cost Index (CEPCI), https://www.chemengonline.com/2019-cepci-updates-january-prelim-and-december-2018-final/; 2019. Accessed 10 July 2019.
47. CBRT (Central Bank of Republic of Turkish), Discount rate and interest rate of Turkey, https://www.tcmb.gov.tr/wps/wcm/connect/TR/TCMB+TR/Main+Menu/Temel+Faaliyetler/Para+Politikasi/Reeskont+ve+Avans+Faiz+Oranlari; 2019. Accessed 10 July 2019.
48. Turton R, Shaeiwitz JA, Bhattacharyya D, Whiting WB. Analysis, synthesis, and design of chemical processes. 5th ed. New Jersey: Prentice Hall; 2018.
49. McCulloch WS, Pitts WA. A logical calculus of the ideas immanent in nervous activity. Bull Math Biophys. 1943;52(1/2):115–33.
50. Abu-Mostafa YS. Neural Networks for Computing?. In: Denker J (eds). Neural networks for computing. New York; Proceedings of the American Institute of Physics Conf.; 1986. pp 1–6.
51. Kargı AVS. Artificial neural network models and application in a textile company. Bursa: Etkin Basım Yayın Dağıtım; 2015 **(in Turkish)**.
52. Oztemel E. Artificial neural networks. Istanbul: Papatya Yayıncılık; 2012 **(in Turkish)**.
53. Fausett L. Fundamentals of neural networks architectures, algorithms and applications. New Jersey: Prentice Hall; 1994.
54. Li Min F. Neural networks in computer intelligence. New York: McGraw-Hill Inc.; 1994.
55. Elmas C. Artificial intelligence applications. 2nd ed. Ankara: Seçkin Yayıncılık; 2010 **(in Turkish)**.
56. MATLAB. The Language of Technical Computing. Version 7.0. U.S.A: The MathWorks Inc.; 2007.